Yu *et al. Soft Sci* 2022;2:5
DOI: 10.20517/ss.2022.04

Soft Science

Review Article

Open Access

Check for updates

Crosslinked organosulfur-based self-assembled monolayers: formation and applications

Tianlang Yu, Maria D. Marquez, Hung-Vu Tran, T. Randall Lee*

Department of Chemistry and the Texas Center for Superconductivity, University of Houston, Houston, TX 77204-5003, USA.

***Correspondence to:** Prof T. Randall Lee, Department of Chemistry, University of Houston, 4800 Calhoun Road, Houston, TX 77204-5003, USA. E-mail: trlee@uh.edu

How to cite this article: Yu T, Marquez MD, Tran HV, Lee TR. Crosslinked organosulfur-based self-assembled monolayers: formation and applications. *Soft Sci* 2022;2:5. https://dx.doi.org/10.20517/ss.2022.04

Received: 24 March 2022 **First Decision:** 11 April 2022 **Revised:** 2 May 2022 **Accepted:** 9 May 2022 **Published:** 27 May 2022

Academic Editor: Zhifeng Ren **Copy Editor:** Jia-Xin Zhang **Production Editor:** Jia-Xin Zhang

Abstract

Self-assembled monolayers (SAMs) have found use in diverse applications that range from corrosion prevention to biosensing. However, for all of these applications, stability remains a key challenge for the utilization of SAMs. Over the last decade, intermolecular crosslinking as a method to enhance the thermal and chemical stability of SAMs has attracted increased attention from scientists and engineers. As such, this review introduces a variety of crosslinked SAMs: (1) aromatic thiol-based SAMs; (2) olefinic- and acetylenic-based alkanethiols; (3) other aliphatic alkanethiols; (4) silane-based alkanethiols; (5) boronic acid-based alkanethiols; and (6) crosslinked SAMs realized by hydrogen bonding. By offering insight into the structure-application relationships of the aforementioned SAMs, this review seeks to inspire researchers toward the development of new classes of SAMs with enhanced stabilities and working lifetimes.

Keywords: Self-assembled monolayers (SAMs), crosslinking, nanocoatings, stabilities, nanostructures

INTRODUCTION

The discovery of the spontaneous adsorption of organic alkane disulfides to metal substrates, such as gold, in 1983 by Nuzzo and Allara as the first example of Self-assembled monolayers (SAMs) and the subsequent use of alkanethiols has led to the widespread use of SAMs[1-3]. Over the past few decades, SAMs have been widely used as a robust surface modification method in various industrial fields, such as in microelectromechanical system (MEMS) devices[4], antifouling coatings for biomaterials[5], and microcontact

© The Author(s) 2022. **Open Access** This article is licensed under a Creative Commons Attribution 4.0 International License (https://creativecommons.org/licenses/by/4.0/), which permits unrestricted use, sharing, adaptation, distribution and reproduction in any medium or format, for any purpose, even commercially, as long as you give appropriate credit to the original author(s) and the source, provide a link to the Creative Commons license, and indicate if changes were made.

printing[6,7]. Compared to conventional polymer coatings, such as polytetrafluoroethylene, SAMs applied onto a surface can be controlled to reach thicknesses in the nanometer range with high uniformity and hydrophobicity[8,9]. For example, silane-based SAMs are routinely applied as nanocoatings in MEMS devices due to their ability to decrease adhesion and friction leading to enhanced performance[10-13].

Compared to normal silane SAMs, which only bind to metal oxides and silicon, thiol-based adsorbates are more compatible with the surfaces of metals, such as gold, silver, and copper, or III-V compounds such as GaAs[14]. As a well-known system, stability has been the major issue that has hindered thiol-based SAMs for further applications. Compared to N-heterocyclic carbenes (NHC)-based SAMs on gold or silane-based SAMs on silicon, which form strong covalent bonds between the adsorbates and substrates, the S-Au interaction is less stable in ambient conditions[15,16]. Previous research has shown that normal alkanethiol SAMs organized by van der Waals (vdW) interaction are sensitive to temperature and desorb from gold surfaces at 70 °C[2,17]. In addition, strong oxidizing reagents damage thin films and produce disulfides in a short period of time.

To broaden the application of SAMs, researchers have put in great effort to develop a more stable SAM system on gold that shows good resistance to high temperatures and harsh chemical conditions. Intermolecular crosslinking is an effective method used to enhance the thermal and chemical stability of SAMs. It is noted that SAM molecules consist of three key parts: the headgroup binding to the corresponding substrate; the methylene spacer, which provides vdW interchain interactions; and the tailgroup[18]. Theoretically, intermolecular crosslinking can occur in all three parts of the SAM molecules. However, unlike the natural formation of a polymerized network for the silane headgroup, the bonding nature of sulfur atoms of thiols determines that crosslinking at the headgroup for thiol-based SAMs is not achievable[19,20].

This review focuses on the crosslinking process of corresponding adsorbates and their applications in materials science. The crosslinked SAMs introduced in this chapter are divided into six categories: (1) aromatic thiol-based SAMs; (2) olefinic- and acetylenic-based alkanethiols; (3) other aliphatic alkanethiols; (4) silane-based alkanethiols; (5) boronic acid-based alkanethiols; and (6) crosslinked SAMs realized by hydrogen bonding [Figure 1].

Table 1 highlights six types of crosslinked SAMs, their corresponding methods of formation, and their potential applications. In contrast to previously published reviews of SAMs, which are largely focused on SAM structures, characterizations, and targeted applications, this review focuses on the stability of crosslinked SAMs and their corresponding applications in materials science. We hope this review will enlighten future advances in nanofabrication and bioengineering.

CROSSLINKED AROMATIC THIOL-BASED SAMS

In 1999, Geyer *et al.*[21] discovered that biphenyl-4-thiol (BPT) can crosslink laterally upon low energy electron irradiation at 50 eV. Additionally, various kinds of SAMs based on aromatic thiols or thiolates can also undergo similar intermolecular crosslinking, which turns the original system into a crosslinked aromatic SAM system [Figure 2][22].

Figure 3[23] summarizes electron-induced crosslinking of aromatic thiol-based SAMs with three different tailgroups compared to *n*-alkanethiol-based SAMs. Unlike the BPT SAMs, which form a crosslinked network under electron irradiation [Figure 3B], normal alkanethiol-based SAMs partially desorb from gold surfaces and form double bonds randomly, as shown in Figure 3A[24,25]. Figure 3C shows that compared to

Table 1. Crosslinked SAMs, their methods of formation, and their potential applications

Crosslinked SAMs	Formation method	Applications
Aromatic thiol-based SAMs	Electron irradiation	1. Electron-beam lithography 2. Surface functionalization 3. Surface-initiated polymerization 4. Carbon nanomembranes (CNMS)
Acetylenic-based alkanethiols	UV irradiation	1. Photolithography 2. Nanoparticles for antifouling 3. Single-layer polydiacetylene fabrication
Aliphatic alkanethiols	Electron irradiation	1. Electron-beam lithography
Silane-based alkanethiols	Hydrolysis	1. Surface-initiated polymerization 2. Surface passivation
Boronic acid-based alkanethiols	Condensation in dry solvents	In development
Crosslinked SAMs realized by hydrogen bonding	Hydrogen bonding	1. Selective binding of cations on surfaces 2. Thermally stable coatings

SAMs: Self-assembled monolayers.

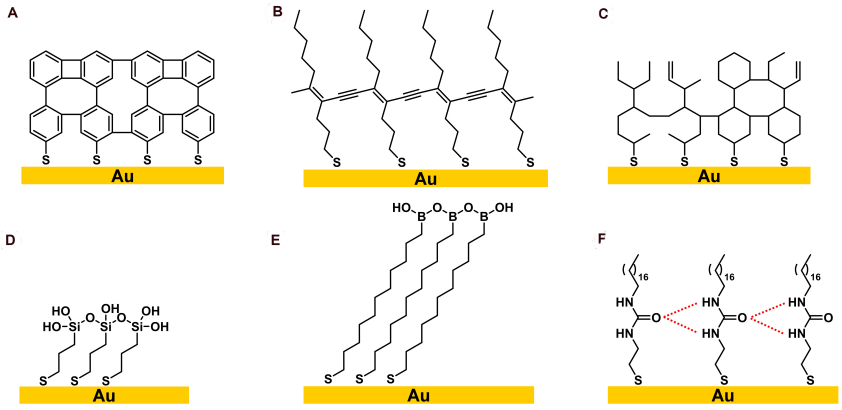

Figure 1. Six different types of crosslinked SAMs: (A) aromatic thiol-based SAMs; (B) acetylenic-based alkanethiols; (C) other aliphatic alkanethiols; (D) silane-based alkanethiols; (E) boronic acid-based alkanethiols; and (F) crosslinked SAMs realized by hydrogen bonding. SAMs: Self-assembled monolayers.

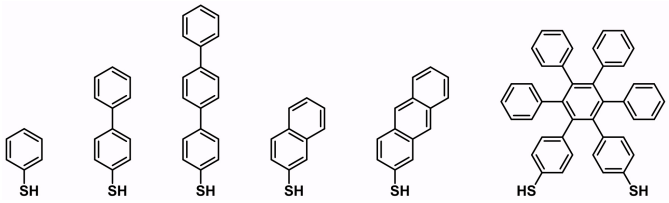

Figure 2. Structures of the precursors used for crosslinked aromatic thiol-based SAMs. Adapted from Ref.[22], copyright 2013 American Chemical Society. SAMs: Self-assembled monolayers.

hydrocarbon aromatic SAMs, nitro-terminated aromatic SAMs not only show crosslinking upon electron irradiation but also have their nitro groups reduced to amino groups[26]. In addition, Zharnikov and co-workers discovered that crosslinking of biphenylthiol SAMs terminated with CH_2NO_2 reduced to SAMs terminated with CH_2NH_2 upon electron irradiation, as shown in Figure 3D[27].

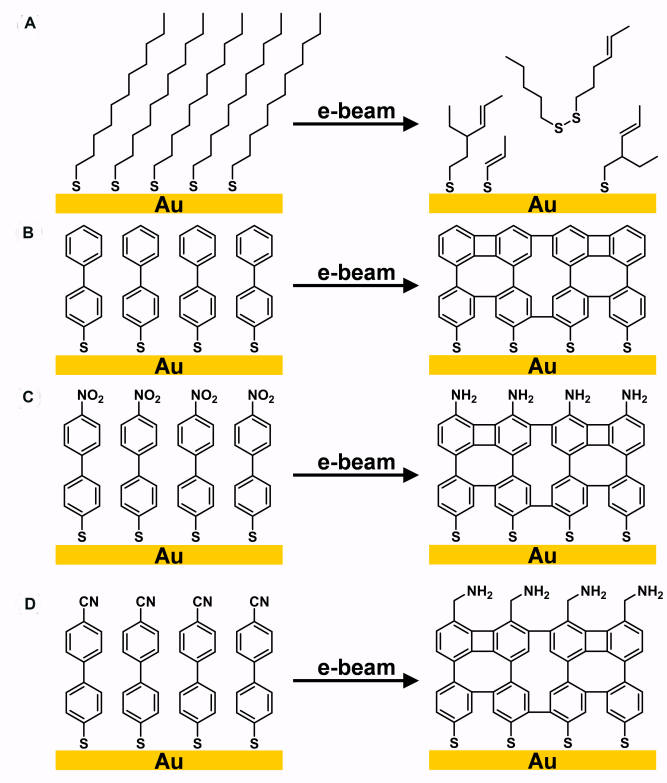

Figure 3. Electron induced crosslinking of (A) aliphatic SAMs; (B) aromatic SAMs; (C) nitro-terminated aromatic SAMs; (D) nitrile-terminated aromatic SAMs. Adapted from Ref.[23], copyright 2012 American Chemical Society. SAMs: Self-assembled monolayers.

Taking BPT SAM as an example, the formation of the crosslinking can be summarized as a dissociative electron attachment (DEA) process [Figure 4][28]. First, under the impact of irradiation, such as electrons or X-rays, a gold substrate emits secondary electrons, as shown in Figure 4A and B[29]. The dissociative primary and secondary electrons lead to C-H bond cleavage of phenyl rings with hydrogen atoms left behind, which yields transient negative ions, as shown in Figure 4C[30]. In this process, the electron affinity of the phenyl radical is 1.1 eV, which is higher than that of hydrogen (0.75 eV)[31]. Thus, the dissociative electron attaches to the phenyl fragment ion instead of hydrogen. The DEA process for benzene is expressed in Equation 1.

$$e^- + C_6H_5{-}H \rightarrow C_6H_5^- + H \quad (1)$$

The key factor for the lateral crosslinked product is the stability of the aromatic backbones, leading to the formation of single and double bonds between the phenyl rings, followed by the release of hydrogen. At the end of the reaction, the lateral crosslinking is terminated by the self-quenching of electron tunneling to the gold surface [Figure 4D][28]. In addition, researchers found that crosslinking of aromatic SAMs also occurs upon exposure to other sources of irradiation such as X-rays (10-100 eV)[32], helium ion beam (HIM, 35 keV)[33], and extreme UV (EUV, 92.5 eV)[34]. These results further confirmed that primary electrons originating from the incoming electron beam are not necessary and that, instead, secondary electrons emitted from the gold surface play a more important role in the crosslinking process.

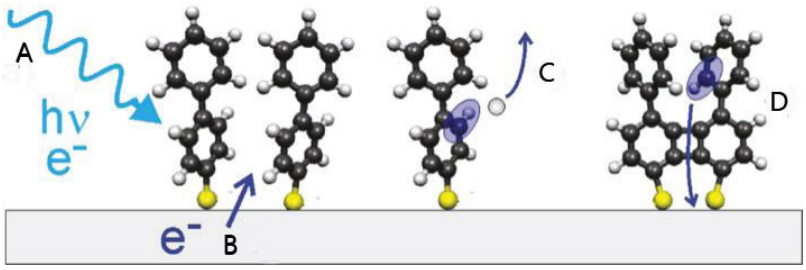

Figure 4. Schematic representation of the different steps involved in the crosslinking of aromatic SAMs: (A) irradiation; (B) emission of secondary electrons; (C) dissociation of C-H bonds; and (D) self-quenching. Reprinted with permission from Ref.[28], copyright 2009 American Chemical Society. SAMs: Self-assembled monolayers.

In addition to irradiation energy, another key parameter for crosslinking aromatic SAMs is the electron dose, which is used to measure the quantity of charge per unit area upon irradiation. Interestingly, there is only a slight difference in crosslinking conditions (electron energy and dose) between extensive SAM precursors. To determine the optimal conditions for irradiation-induced crosslinking, scientists have used the cross section, σ, as a parameter to gauge when a rate reaches saturation behavior[35]. The cross section for the electron irradiation involves a balance between the crosslinking degree of the SAMs and the damage to the gold interface, which is determined as the primary electron energy of 50 eV[30]. Recently, Koch and co-workers investigated the crosslinking efficiency of halogenated biphenyl thiols[36]. The authors found that iodide-substituted biphenyl thiol showed more efficient electron-induced crosslinking than fluorine- or bromine-substituted species. Moreover, the electron dose determines the degree of crosslinking, and the crosslinking degree of the SAMs increases with the electron dose, reaching a maximum of ~90% at an electron dose of ~50 mC/cm^2 and above, as determined by X-ray photoelectron spectroscopy (XPS)[37]. However, completely crosslinked SAMs are not achievable because of the steric effect of the biphenyl structure[28]. Upon irradiation at higher doses, no further change to the resulting film itself is observed, but the gold interface is damaged, and crosslinked films are desorbed from surfaces[37].

Compared to the pristine BPT SAM, infrared (IR) spectra for the crosslinked product show that two peaks arising from the C-H stretching vibration of the pristine phenyl ring at 3046 cm^{-1} and 3038 cm^{-1} disappear after electron irradiation. Figure 5 shows the XPS spectra for the C 1s and S 2p regions of (A) biphenyl-terminated SAMs and (B) terphenyl thiol SAMs following electron irradiation (50 eV, 60 mC/cm^2)[22]. In the C 1s region, the integrated C 1s peak decreases in both of the SAMs investigated after crosslinking. The carbon content in the biphenyl-terminated SAM with hydrocarbon chains is decreased by 16%, and the calculated thickness is decreased from 12 Å to 10 Å, as determined by XPS. To explain these results, Schnack and co-workers performed a molecular dynamics simulation for crosslinking various biphenyl-terminated SAMs, which indicated that partial dissociation of the aromatic rings takes place to maximize the 2D molecular network[38]. In the XPS spectra obtained for S 2p, pristine SAMs exhibit a characteristic peak due to bound thiols (red lines), which appears as a doublet (S $2p_{3/2}$ and S $2p_{1/2}$) at binding energies of 162.0 eV and 163.0 eV, respectively[39]. The new peak appearing at 163.5 eV for the crosslinked SAMs suggests the formation of unbound sulfur species or disulfides because of the cleavage of S-Au bonds after irradiation, as shown by the green line obtained by spectral deconvolution. The results obtained from low-energy electron diffraction and a scanning tunneling microscope (STM) also indicate a loss of long-range order in the crosslinked aromatic SAMs.

Applications

Electron-beam lithography

In the modern semiconductor industry, lithography is one of the basic processes used for transferring a

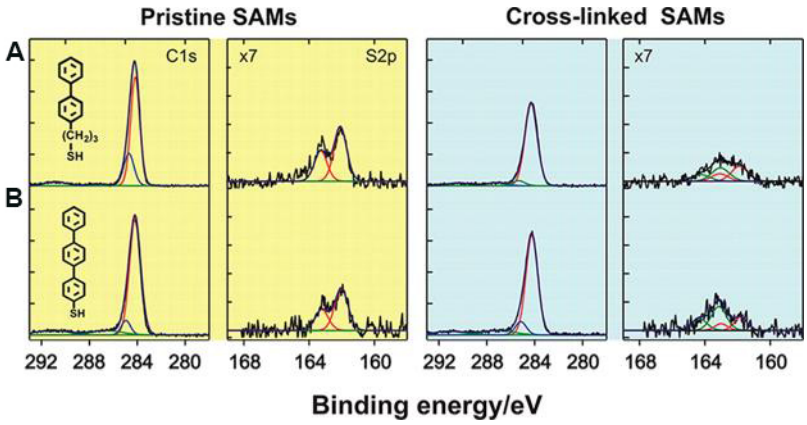

Figure 5. XPS data for pristine and crosslinked SAMs. XPS spectra for C 1s and S 2p regions of pristine (in yellow) and electron irradiated (50 eV, 60 mC/cm^2) monolayers (in blue) of (A) biphenyl-terminated SAM, (B) terphenyl thiol SAM. Adapted from Ref.[22], copyright 2013 American Chemical Society. XPS: X-ray photoelectron spectroscopy; SAM: self-assembled monolayer.

designed pattern onto semiconductor substrates, followed by an etching or metal deposition process to fabricate microelectronic devices[40]. Mainstream lithography techniques include photolithography, electron-beam (e-beam) lithography, and ion-beam lithography[41]. In the case of e-beam lithography, surface patterning is achieved by directly controlling an electron beam to write onto a resist-coated surface[42]. There are two types of e-beam resists in e-beam lithography: positive and negative. With a positive resist, the areas exposed to the e-beam are removed by a developer solution in the next step to expose the bare substrate. In contrast, for a negative resist, only the areas of the resist exposed to the e-beam remain, while the other areas are removed[43]. To fabricate a high resolution and high aspect ratio pattern on a surface, the negative resist used in e-beam lithography needs to have high sensitivity to electrons, small molecular size, and low thickness[44].

When the crosslinked BPT SAMs were first discovered by Geyer and co-workers in 1999, the authors noted that these crosslinked SAMs showed good resistance to chemical etching solution[21]. Compared to a conventional polymeric resist such as polymethylmethacrylate (PMMA), crosslinked aromatic SAMs have the potential to be used as negative resists in e-beam lithography. To test BPT SAMs for use as negative resists, Hinze and co-workers patterned BPT-coated gold substrates with an e-beam. Then, the patterned SAM-coated surface was placed into a 0.2 M KCN/1 M KOH solution for chemical etching, also called a wet etching process. After wet etching, the gold surface with crosslinked SAMs remained while the other pristine SAM areas were etched away, which showed clear patterns with a depth of 20 nm and small width of down to 10 nm [Figure 6][45].

Subsequently, Yildirim and co-workers investigated the lithography properties of crosslinked aromatic SAMs containing one, two, and three phenyl rings[37]. The BPT SAM exhibits the best performance as a negative resist, as the phenyl thiol fails to form a highly crosslinked network, and the pristine terphenyl thiol SAMs are hard to remove by wet etching. Fluorinated SAMs (FSAMs) have been used for surface modification thanks to the excellent hydrophobic and low surface friction properties of fluorinated materials[46]. However, FSAMs are vulnerable to radiation damage by low-energy electrons[47]. To solve this issue, Terfort and co-workers investigated crosslinked perfluoroterphenyl-terminated SAMs exposed to low-energy electrons with a low dose (10 eV, 30 mC/cm^2), as shown in Figure 7[48]. Note that the cleavage of C-F bonds observed upon irradiation follows the behavior of hydrocarbon aromatic SAMs. Additionally, the crosslinked FSAMs can be used as e-beam resists and hydrophobic coatings.

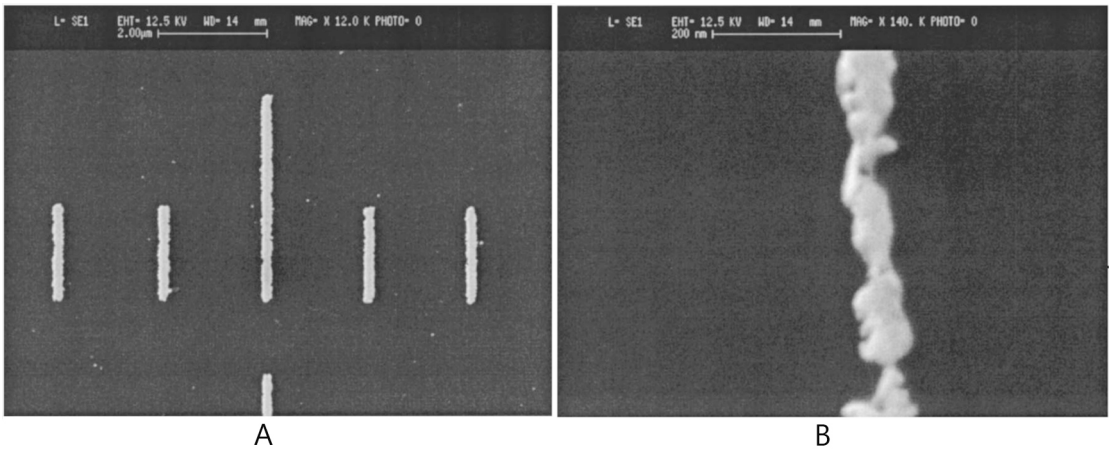

Figure 6. SEM image of lines with a width of: (A) 100 nm, (B) 10 nm prepared using a BPT SAM negative resist. Reprinted with permission from Ref.[45], copyright 2000 AVS. BPT: Biphenyl-4-thiol; SAM: self-assembled monolayer.

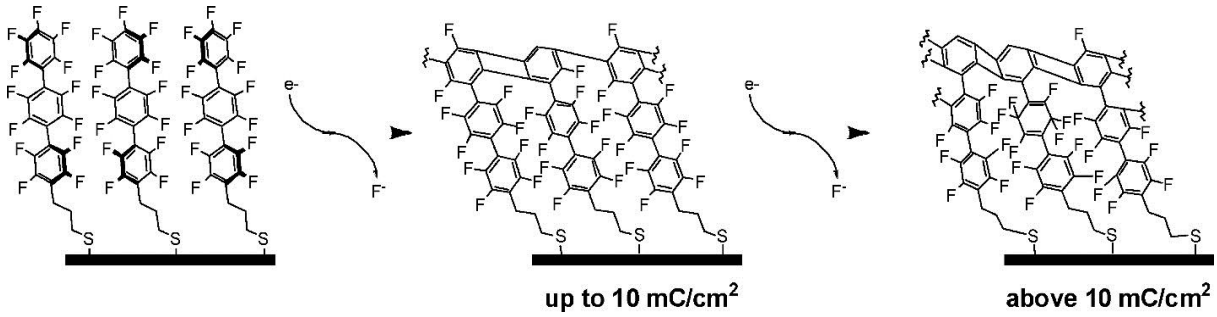

Figure 7. Schematic representation of electron-induced crosslinking of perfluoroterphenyl-terminated SAMs. Reprinted with permission from Ref.[48], copyright 2009 American Chemical Society. SAMs: Self-assembled monolayers.

In summary, BPT SAM and its derivatives have been widely used in e-beam lithography[23]. Chemical etching, direct laser patterning[49], thermodesorption[50], and SAM exchange[34,51] can be used to remove pristine SAMs on a surface to form a pattern. All the methods mentioned above utilize the high stability of crosslinked SAMs compared to pristine SAMs.

Surface functionalization

Surface functionalization plays an important role in biotechnology applications. By modifying a surface with different chemical functional groups, researchers can immobilize and detect biomolecules efficiently[52]. In 2007, Turchanin and co-workers crosslinked 4'-nitro-4-biphenylthiol (NBPT) through a stencil mask to fabricate a patterned amino-terminated SAM, as shown in Figure 8A[34,53]. XPS spectra show that after irradiation, the peak in the N 1s region shifts from 405.5 eV to 399.2 eV and the peak intensity in the O 1s region decreases significantly, which represent the full reduction of amino functional groups from nitro functional groups, as shown in Figure 8B.

In a follow-up study, an NBPT SAM was used for the fabrication of a protein microarray for biodetection applications[54,55]. The NBPT SAM on gold was crosslinked by e-beam irradiation through a stencil mask. The remainder of the pristine NBPT SAM was exchanged with protein-resistant SAMs terminated with an ethylene glycol segment[56]. Finally, a chelator was added to the surface, followed by drop-casting of a protein solution, as shown in Figure 9A. Thanks to the strong binding between amino groups and the target

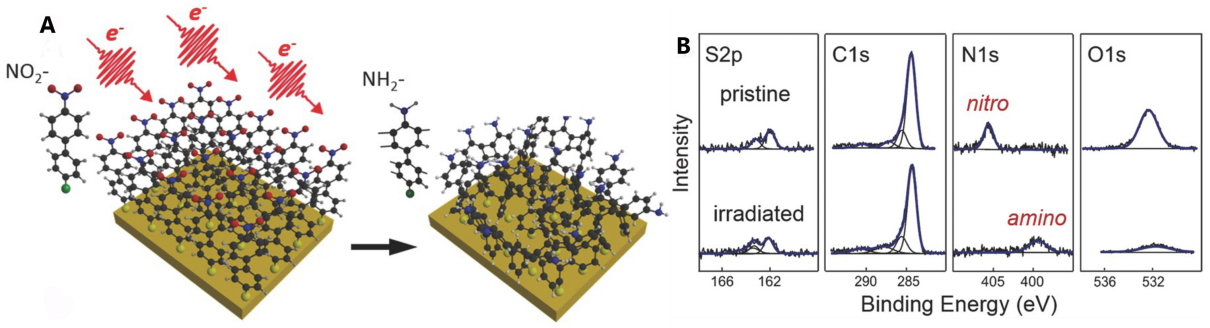

Figure 8. Irradiation-induced crosslinked NBPT SAM. (A) Schematic representation of the irradiation process, (B) XPS spectra for NBPT on gold before and after irradiation. Reprinted with permission from Ref.[53], copyright 2016 Wiley. NBPT: 4'-nitro-4-biphenylthiol; SAM: self-assembled monolayer; XPS: X-ray photoelectron spectroscopy.

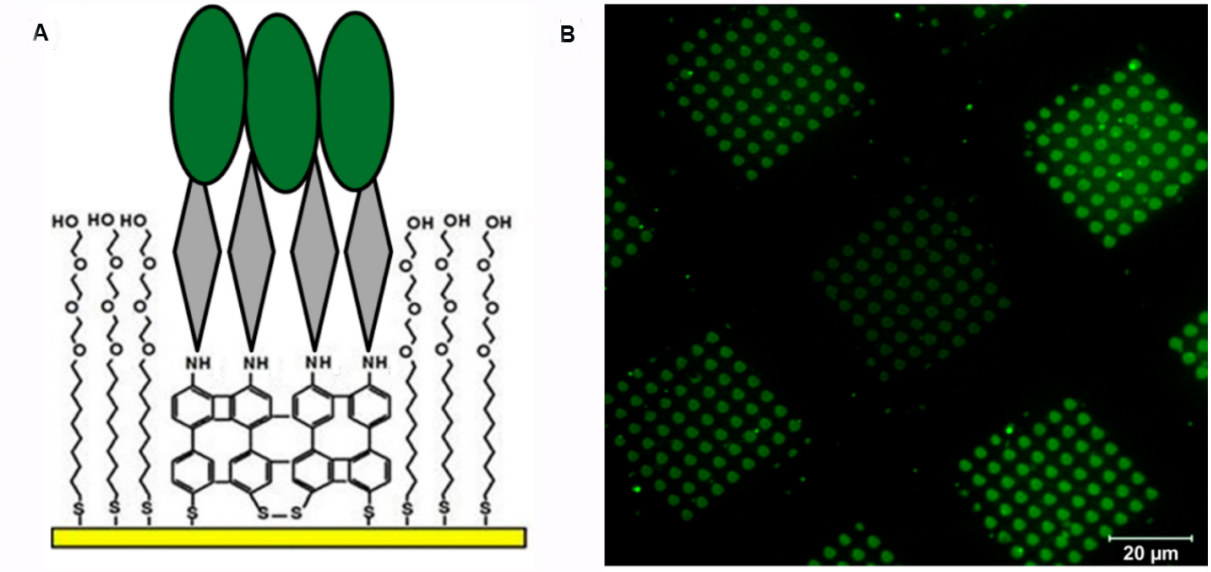

Figure 9. (A) A schematic of the protein microarray structure. (B) Laser scanning microscopy (LSM) image of a protein microarray fabricated by a crosslinked NBPT SAM. Adapted from Ref.[54], copyright 2017 American Chemical Society. NBPT: 4'-nitro-4-biphenylthiol; SAM: self-assembled monolayer.

protein, only the electron-irradiated areas were covered with proteins that showed strong fluorescence, as demonstrated in Figure 9B[54]. Nitrile-terminated aromatic SAMs, which also reduce to amino-terminated crosslinked SAMs upon irradiation, have been investigated by Zharnikov and co-workers[27]. Researchers found that compared to the NBPT SAM, cyanobiphenyl thiol forms less dense amino groups on the surface after irradiation due to partial defragmentation of tailgroups. For the aforementioned crosslinked perfluoroterphenyl-terminated SAMs, researchers have adopted this system for metal deposition for electronic applications, which utilize crosslinked films to prevent the intercalation of metal atoms[57].

Surface-initiated polymerization

Surface-initiated polymerization (SIP) shows promise for protective coating applications, such as antifouling and anti-corrosion[58]. Recently, the NBPT SAM has attracted more and more attention in this application because of its precise control of polymer growth in selective areas with nanometer resolution[59,60]. In this method, NBPT SAM was patterned by e-beam lithography, resulting in a stable

crosslinked amino-terminated SAM, as shown in Figure 10A and B. Next, the amino tailgroups were converted to diazo initiators in a diazotization process, as shown in Figure 10C. Finally, as shown in Figure 10D, the polymerization was started by adding styrene monomer and catalyst to the solution. After photopolymerization, electron-irradiated SAM areas yielded polystyrene (PS) brushes with a minimum thickness of 10 nm[60]. In a follow-up study, by combining a crosslinked NBPT SAM and various monomers, researchers grew homogeneous polymer brushes with thicknesses ranging from 10-300 nm precisely, which respond to pH changes and can be used for building microsensors[61].

Carbon nanomembranes (CNMS)

In 2005, Gölzhäuser and co-workers fabricated the first carbon nanomembranes (CNMs) from crosslinked aromatic SAMs[62]. As shown in Figure 11A and B, after the crosslinked aromatic SAMs were formed on the surface of gold, a transfer medium, PMMA, was coated on top of the SAMs. Then, the gold surface was etched as a sacrificial substrate to release the crosslinked films. Finally, CNMs were transferred onto other substrates, such as metal grids, Si, and graphene, followed by dissolution of the PMMA, as shown in Figure 11C and D.

Since CNMs are converted from aromatic SAMs, their physical properties, such as thickness, rigidness, and porosity, can be tailored by using different SAM precursors[63]. Figure 12 shows helium-ion microscopy images of CNMs obtained from six different SAMs on TEM grids. From Figure 12A-C, the thickness of the pristine SAMs increases from 0.6 nm to 2.4 nm, resulting in the final thickness of the CNMs increasing accordingly. Moreover, while the use of a small SAM molecule such as that shown in Figure 12D leads to hole-free CNMs, bulkier molecules (such as the molecules in Figure 12E and F) form less-ordered SAMs and create more porous CNMs due to lower packing densities and intermolecular stacking[22]. Additionally, it is simple to pattern CNMs with uniform nanoholes as nanosieves using e-beam lithography[64].

Furthermore, CNMs are easily chemically functionalized by using SAM precursors with different functional groups, as used for coupling biomolecules and polymers[65]. After amino-terminated CNMs are released from gold, the thiol group on the opposite site of the CNM can couple with Au nanoparticles or other functional groups such as maleimide to form a Janus nanomembrane[66]. After years of rapid development, CNMs prepared from crosslinked aromatic SAMs have various applications in many fields, such as graphene manufacturing[67], nanofiltration[68], and microdetectors[69,70].

In 2013, Turchanin and co-workers grew single-layer graphene on Cu by annealing CNMs at above 800 °C for 2 h, as shown in Figure 13A[71]. The authors continued this research and fabricated patterned graphene from CNMs by using e-beam lithography[72]. From XPS spectra shown in Figure 13B, a doublet was observed at a binding energy of 161.2 eV (blue line), which was attributed to copper sulfides, and a doublet due to bound thiolate (red line) was found to completely disappear after annealing. Interestingly, the S 2p signal in the XPS spectra completely disappeared after transferring graphene to a Si-wafer, which indicated S-C bond cleavage and that sulfur atoms were left on the Cu substrate. After annealing BPT CNM into graphene, Young's modulus was found to increase from 10 GPa to 48 GPa, indicating a significant increase in the mechanical strength[73].

For separation, thin membranes, which combine high permeability and high selectivity, are desirable in the water treatment industry[74,75]. CNMs and graphene can be fabricated into layers as thin as 1 nm, with a nanoporous structure and excellent mechanical strength, which make them excellent candidates for nanofiltration[76,77]. Furthermore, researchers have used amino-terminated CNMs to stack graphene to fabricate CNM/graphene field-effect transistors (FETs) as an alternative for graphene functionalization for

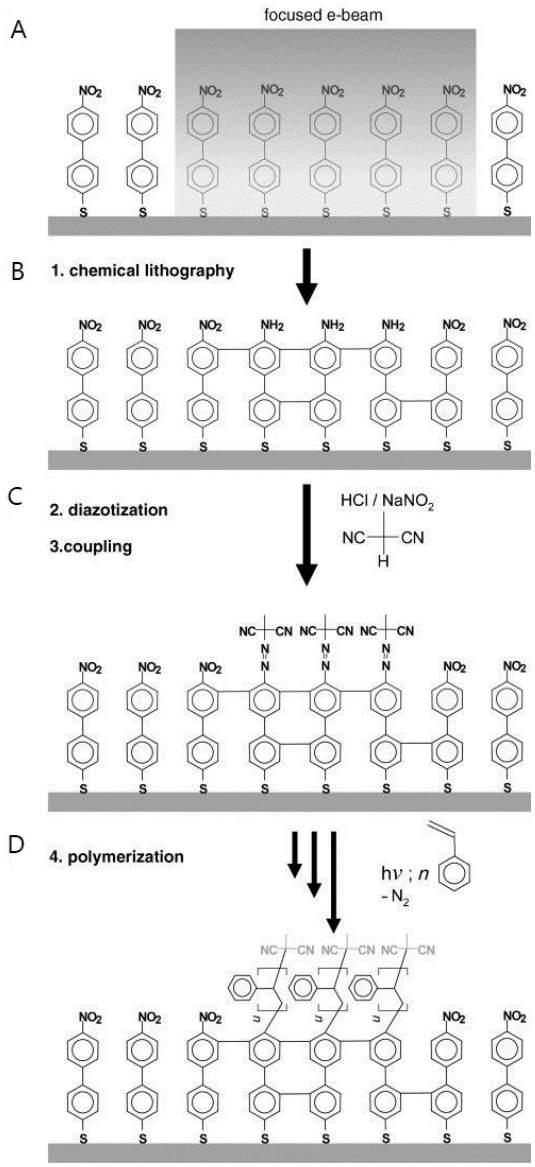

Figure 10. Schematic representation of polymer brush fabrication. Reprinted with permission from Ref.[60], copyright 2007 Wiley.

biosensors and gas sensors[69,70].

CROSSLINKED OLEFINIC- AND ACETYLENIC-BASED SAMS

Beside crosslinked aromatic thiol-based SAMs, crosslinked SAMs from olefinic- and acetylenic-based alkanethiols have also been well studied by scientists. Additionally, polydiacetylene materials are a type of conducting polymer with special optical properties that have extensive applications in photonics, nanoelectronics, and biosensors[78]. When polydiacetylene materials couple with chemical and biological stimuli, their characteristic absorption peak shows a redshift. Therefore, they have a sensitive chromic response to microorganisms, viruses, and proteins, which is attractive for biosensing applications[79].

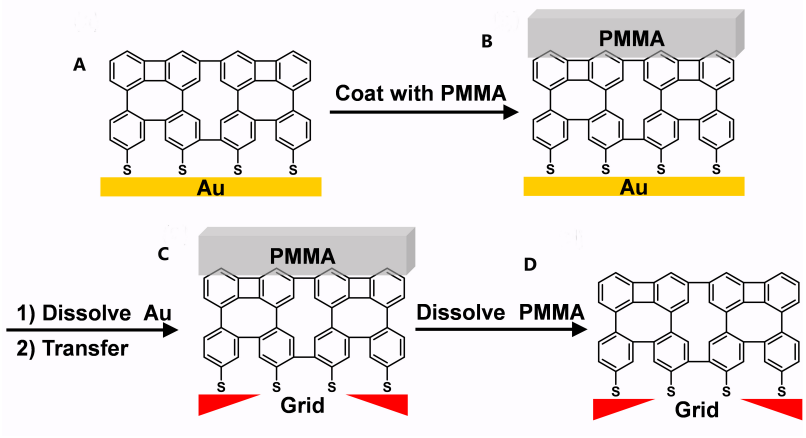

Figure 11. Schematic representation of the transfer of CNMs onto other surfaces such as metal grids. Adapted from Ref.[23], copyright 2012 Elsevier. CNMs: Carbon nanomembranes.

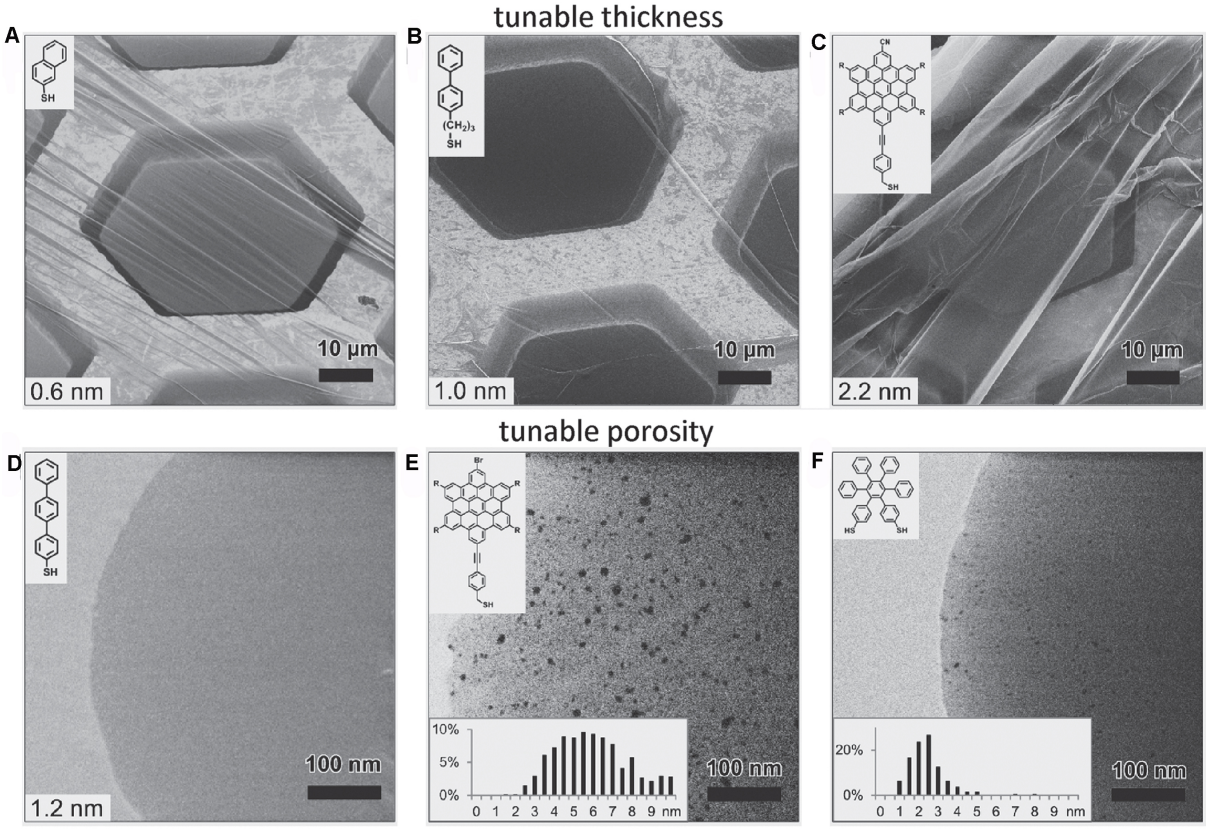

Figure 12. HIM images of CNMs converted from various pristine SAMs and then transferred onto TEM grids. The upper left insets show the pristine SAMs. Adapted from Ref.[22], copyright 2013 American Chemical Society. HIM: Helium ion beam; CNMs: Carbon nanomembranes; SAMs: self-assembled monolayers.

Crosslinked SAMs containing polydiacetylene were first reported by Batchelder *et al.*[80] in 1994. The authors deposited polymeric monolayers from diacetylene-containing disulfide onto Au (111) surfaces, as shown in Figure 14. Similar to diacetylenes in the solid-state, the chain polymerization of diacetylene thiolates (DATs) on surfaces follows some spatial conditions: the distance of the adjacent thiolates is 4.7-5.2 Å, and the

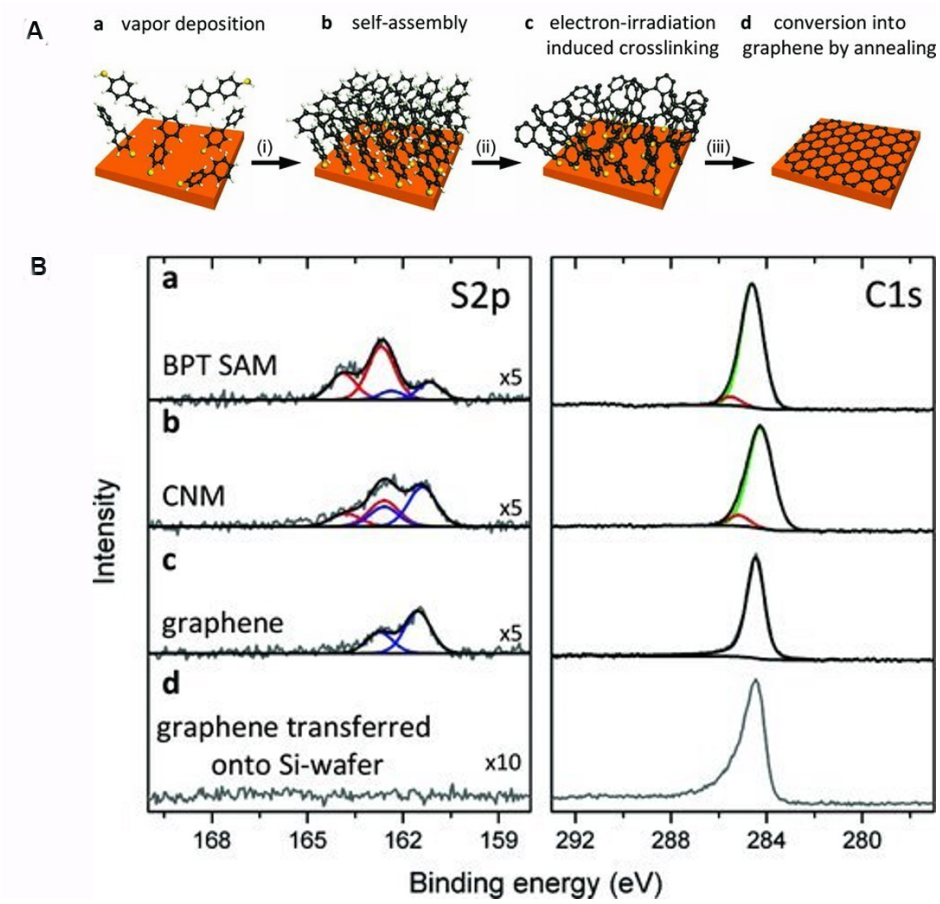

Figure 13. Conversion of BPT SAMs into graphene on copper substrates: (A) Schematic representation, (B) XPS spectra for the products in each step. Adapted from Ref.[71], copyright 2013 Wiley. BPT: Biphenyl-4-thiol; SAMs: self-assembled monolayers; XPS: X-ray photoelectron spectroscopy.

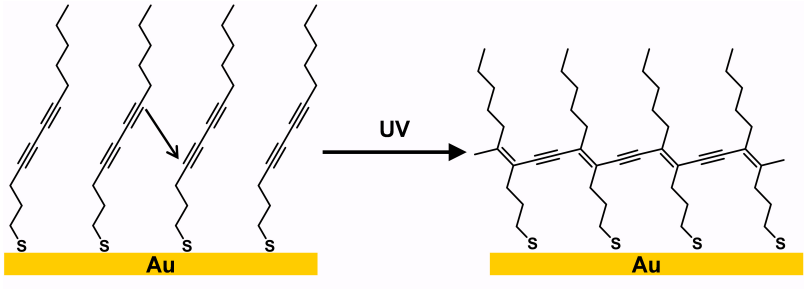

Figure 14. Schematic representation of the polymerization process of DATs on Au. Adapted from Ref.[81], copyright 1999 American Chemical Society. DATs: Diacetylene thiolates.

distance between the C1 carbon of one diacetylene group to the C4 carbon of the adjacent diacetylene group (black arrow in Figure 14) is 3.4-4.0 Å[81,82]. In contrast, diacetylenes undergo both 1,2- and 1,4-polymerization in solution.

The mechanism for 1,4-photopolymerization of diacetylenes is illustrated in Figure 15[82]. First, the initiation is started by UV irradiation of DAT monomers, which generates a diradical monomer, as shown in

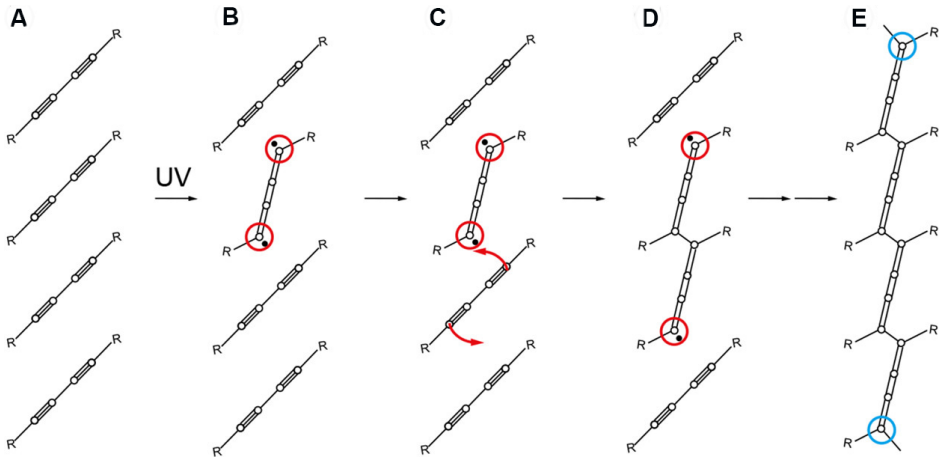

Figure 15. Mechanism for 1,4-photopolymerization of diacetylenes. (A) Array of diacetylene molecules. (B) An excited diradical monomer (red circles). (C) Coupling of the neighboring monomer (red arrows). (D) Diradical dimer. (E) Chain propagation reaction toward both sides until termination of reactive radicals (blue circles). Reprinted with permission from Ref.[82], copyright 2019 American Chemical Society.

Figure 15A and B. After that, an addition reaction occurs at both ends of the diradical monomer, as shown in Figure 15C. Finally, chain propagation at both sides [Figure 15D] is followed by the termination of reactive radicals, as suggested by the blue circles in Figure 15E. The polydiacetylene backbone contains alternating double and triple bonds, which are represented in a resonance structure of three cumulative double bonds, as shown in Figure 15E.

In a following study, Cai *et al.*[81] investigated the influence of ultraviolet (UV) exposure time on the crosslinked product. They used resonance Raman spectroscopy to monitor the polydiacetylene backbone in crosslinked SAMs as a function of UV exposure time, which showed that the effective conjugation length in crosslinked DAT SAMs reached a maximum at 7 min before decreasing. This might be due to the increase in the hybridization strain in the polydiacetylene backbone as well as in the methylene chains with prolonged UV exposure. Batteas and co-workers studied the properties of crosslinked dodeca-4,6-diyne-1-thiol (C3-DATs)[83]. Figure 16A shows the ATR-FTIR spectra obtained for C3-DATs and C3-poly-DATs on Au (111) surfaces. In both spectra for C3-DATs and C3-poly-DATs, the peaks at ~2923 cm^{-1} and ~2854 cm^{-1} are attributed to a methylene asymmetric and symmetric stretching band, respectively. After polymerization, a decrease in both peak intensities is observed without the peak position shifting, which is due to the decrease in the tilt angle of the alkyl chains. As shown in Figure 16B, two new peaks at ~1875 cm^{-1} and ~2450 cm^{-1} for C3-poly-DATs are observed in the Raman spectra. These two peaks can be attributed to the new double and triple bonds formed in the product films, which further confirms the polymerization of the DAT SAMs.

In a separate study, Menzel *et al.*[84] studied the effect of the diacetylene functional group position on crosslinked DAT SAMs. They discovered that moving the diacetylene moiety closer to the thiol headgroup increases the hybridization strain in the alkyl chain, which reduces the conversion of polymerization. In addition, with carboxylic acid-terminated DATs on Au (111), researchers were able to convert carboxylic acid into acid chloride, followed by coupling with other DATs to fabricate double and multilayer polydiacetylene coatings[85]. By using this method, scientists utilized carboxylic acid-terminated DATs as scaffolds to build polydiacetylene thin films layer-by-layer, up to a thickness of 6 layers. The authors subsequently synthesized DAT SAMs on Au (111) with terminal methyl, hydroxyl, and carboxyl acid functional groups[86]. Compared to normal alkanethiol SAMs or pristine DAT SAMs on Au surfaces, all

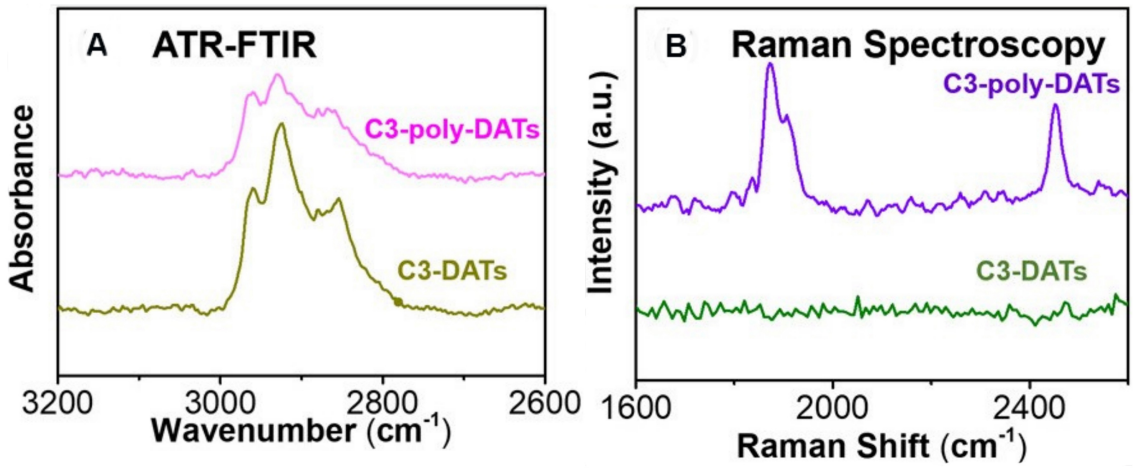

Figure 16. (A) ATR-FTIR and (B) Raman spectra for C3-DATs and C3-poly-DATs on Au (111) surfaces. Adapted from Ref.[83], copyright 2020 American Chemical Society. DATs: Diacetylene thiolates.

crosslinked DAT SAMs showed excellent stability toward repeated electrochemical cycling, high temperatures of up to 200 °C, and basic solutions[86].

Another type of crosslinked SAM derived from olefinic-based alkanethiols is mercaptomethyl styrene, which was discovered by Schlenoff and co-workers in 1996[87]. In this case, polymerization of the absorbates was initiated by immersing the substrate in an azo initiator solution at 58 °C or by irradiating with a green laser [Figure 17]. Time-resolved SERS spectra showed a peak at 1625 cm^{-1} that disappeared after crosslinking, which was attributed to the double bonds of the pristine SAM.

Applications

Photolithography

Crosslinked DAT SAMs have many applications in photolithography, SAM-coated nanoparticles, and single-layer polydiacetylene fabrication. Photolithography is one of the most widely used techniques in semiconductor fabrication, which transfers patterns by exposing photoresist-coated surfaces to UV through a photomask[40]. In 1995, Crooks and co-workers applied UV irradiation to a DAT SAM-coated Au (111) to fabricate patterned polydiacetylene thin films[88]. The uncrosslinked portion of the DAT SAM was stripped using electrochemical desorption, followed by KCN/KOH solution etching. STM depth profiles indicated that a clear negative pattern was formed on the Au (111), which was approximately 7-8 nm in depth. These results validated the use of DAT SAMs as ultra-thin photoresists, which crosslink under UV and protect the underneath surfaces.

Nanoparticles for antifouling

In addition to application as a negative resist in photolithography, crosslinked DAT SAMs are valuable in SAM-coated nanoparticles in biomedical applications. In 2014, Jiang and co-workers coated gold nanoparticles with SAMs containing diacetylene to test their stability in different complex media, as shown in Figure 18[89]. The carboxybetaine functional group is one of the zwitterions that are used for antifouling coatings[90]. The authors designed and synthesized carboxybetaine-terminated alkanethiol with photocrosslinkable diacetylene in the alkyl chain spacer, and then crosslinked it on gold nanoparticles using UV irradiation to enhance the antifouling property. The crosslinked SAM-coated gold nanoparticles showed high resistance to protein fouling from blood serum and decreased cell uptake. Additionally, they

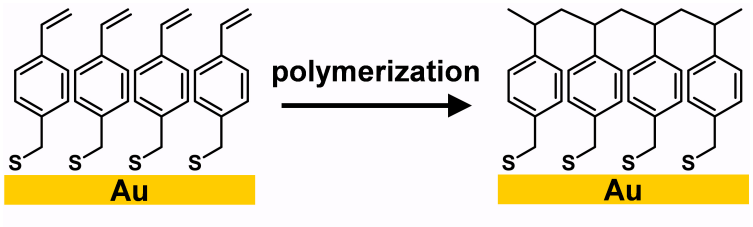

Figure 17. Schematic representation of the polymerization of MMS on Au. Adapted from Ref.[87], copyright 1996 American Chemical Society. MMS: Mercaptomethyl styrene.

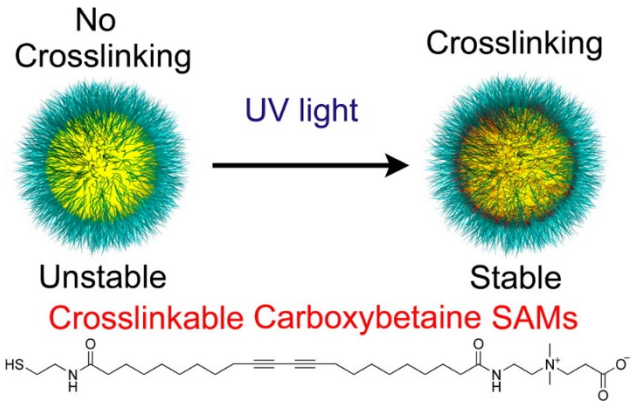

Figure 18. A schematic showing cross-linked gold nanoparticles with CBSH-X. Reprinted with permission from Ref.[89], copyright 2014 American Chemical Society.

were stable at low/high pH and a high temperature of 80 °C.

Single-layer polydiacetylene fabrication

Recently, Wang *et al.*[91] invented a new strategy to fabricate single-layer polydiacetylene thin films using a SAM-coated gold electrode as a template. As illustrated in Figure 19, the authors deposited a functionalized gold electrode with dodecanethiol (DT), followed by the assembly of pentacosa-10,12-diynoic acid via an electrode potential, which formed a well-ordered second monolayer on the DT. After photopolymerization by UV, the polymerized monolayer of polydiacetylene was desorbed by application of an opposite electrode potential, which repeatedly worked to produce 2D polydiacetylene thin films.

OTHER CROSSLINKED ALIPHATIC SAMS

In contrast to the crosslinking of aromatic thiol-based SAMs, aliphatic thiol-based SAMs undergo decomposition and disordering upon electron irradiation[92-95]. Interestingly, in the case of 4-cyclohexylcyclohexanethiols (CCHT), a cyclic aliphatic thiol-based SAM on Au (111), the irradiation-induced crosslinking process was found to be dominant over defragmentation and desorption[96].

Until now, the only study of irradiation-induced crosslinking of cyclic aliphatic thiol-based SAMs was reported by Zharnikov[96] and co-workers in 2012. The authors found that both SAMs generated from *trans*- and *cis*-conformations of CCHT crosslinked upon exposure to electron radiation, as shown in Figure 20. This contrasts with the linear aliphatic thiol-based SAMs, which were severely damaged when exposed to quite low irradiation doses (5-8 mC/cm^2).

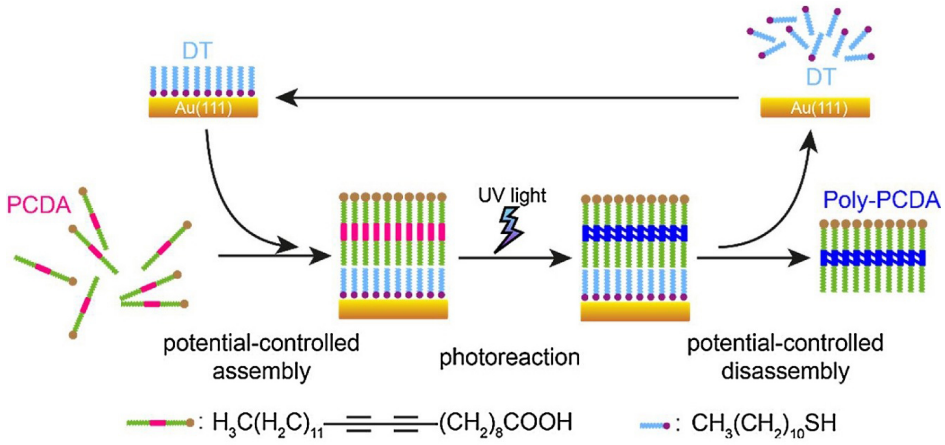

Figure 19. Schematic representation of the fabrication of single-layer polydiacetylene through co-assembled PCDA and DT double layers. Reprinted with permission from Ref.[91], copyright 2017 Elsevier. PCDA: Pentacosa-10,12-diynoic acid; DT: dodecanethiol.

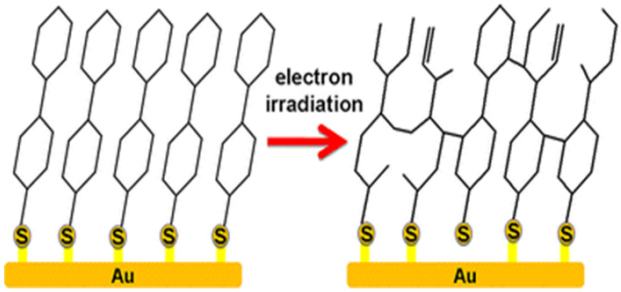

Figure 20. The formation of a crosslinked SAM of CCHT via electron irradiation. Reprinted with permission from Ref.[96], copyright 2012 American Chemical Society. SAM: Self-assembled monolayer; CCHT: 4-cyclohexylcyclohexanethiols.

Under electron irradiation conditions, the C-H bonds are cleaved to generate radical moieties, which are relatively stable because of the nature of the cyclic skeletons of CCHT before crosslinking to other absorbates to form a 2D molecular network. Compared to the linear aliphatic thiol SAMs, the presence of cyclic rings is the key to the dominance of crosslinking over fragmentation and desorption processes. In cases where the C-C bonds belonging to the cyclic rings are cleaved, both fragments were still attached to the molecule matrix, which then, subsequently form cross-linked bonds with neighboring molecules. Hence, the desorption of fragments is suppressed. The newly formed 2D network by crosslinking also hinders the cleavage of the headgroup-substrate S-Au bonds.

Applications

Electron-beam lithography

Similar to aromatic SAMs, crosslinked CCHT SAMs have been used as negative resists in e-beam lithography[96]. Figure 21 shows the SEM images of gold surfaces patterned using SAMs as resists: (A) *cis*-CCHT; (B) *trans*-CCHT; and (C) dodecanethiol (DDT). While the crosslinked SAMs composed of *cis*- and *trans*-CCHT were found to protect the irradiated areas and the nonirradiated areas were efficiently etched, the irradiation-induced damage to the DDT-based SAMs allowed preferred etching of the irradiated areas.

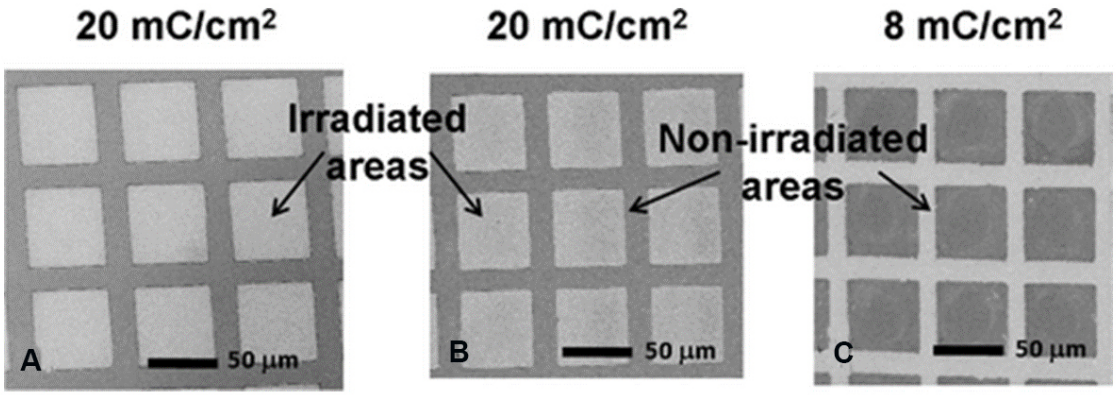

Figure 21. The SEM images of Au surfaces patterned using SAMs as resists: (A) *cis*-CCHT; (B) *trans*-CCHT, and (C) DDT. Reprinted with permission from Ref.[96], copyright 2012 American Chemical Society. CCHT: 4-cyclohexylcyclohexanethiols; DDT: dodecanethiol.

CROSSLINKED SILANE-BASED SAMS

Another important type of crosslinked SAMs are silane-based alkanethiols, which can be used in SIP[97], surface passivation[98,99], and anti-corrosion coatings[100,101]. The crosslinked silane network forms a dense film to prevent oxygen or moisture from diffusing into interfaces, which provides for long-term surface passivation. Additionally, the high thermostability of the crosslinked SAMs helps one to grow polymer brushes at high temperatures in applications involving SIP[97].

As a pristine molecule for crosslinked silane-based alkanethiols, (3-mercaptopropyl) trimethoxysilane (MPTMS) has been well studied and widely adopted in the aforementioned applications. Taking MPTMS SAM as an example, as shown in Figure 22, the formation of a crosslinked MPTMS SAM can be concluded in 3 steps: (1) MPTMS molecules are deposited onto a gold surface in anhydrous conditions to avoid self-polymerization; (2) hydrolysis of the silane converts the methoxy group (-OCH_3) connected to Si to hydroxyl groups (-OH) in the presence of water; (3) at the same time, intermolecular condensation leads to the Si-O-Si structure forming a crosslinked polysiloxane network[102,103]. It should be noted that the trimethoxysilane group is less reactive to water than the trichlorosilane group, making it easier to control the polymerization of the silane on a surface[16]. In this stage, with silanol groups present on the surface, one can generate thick self-polymeric films[98] or enable grafting onto other silanes with specific functional groups[97].

Applications

Surface-initiated polymerization

In 1994, Aramaki and co-workers coated hydroxyl-terminated alkanethiols onto a copper surface, followed by deposition of alkyltrichlorosilane[104]. The hydroxyl groups coupled with alkyl trichlorosilane resulted in a film with a crosslinked polysiloxane network. In 2011, Baker and co-workers used silane-based alkanethiols to fabricate crosslinked atom transfer radical polymerization (ATRP) initiators to grow polymer brushes on gold, as shown in Figure 23[97]. After the crosslinked MPTMS SAM was formed on Au to provide a hydroxylated surface, another silane terminated with an initiator was grafted onto the MPTMS SAM, which formed a second layer of crosslinked interchain polysiloxane. After adding methyl methacrylate monomer and catalyst, the system was heated up from 50 °C to 100 °C to initiate polymerization of PMMA from Au surfaces.

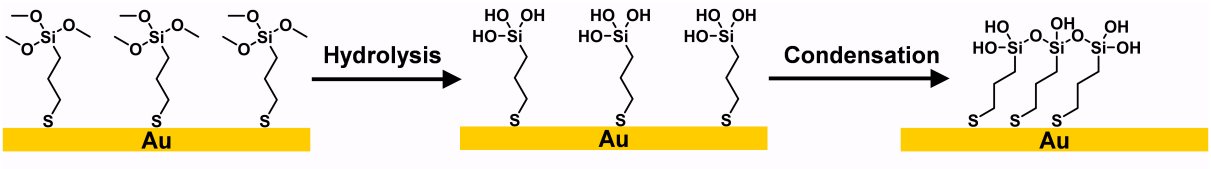

Figure 22. Schematic representation of crosslinked MPTMS SAM formation on Au. Adapted from Ref.[102], copyright 2016 American Chemical Society. MPTMS: (3-mercaptopropyl) trimethoxysilane; SAM: self-assembled monolayer.

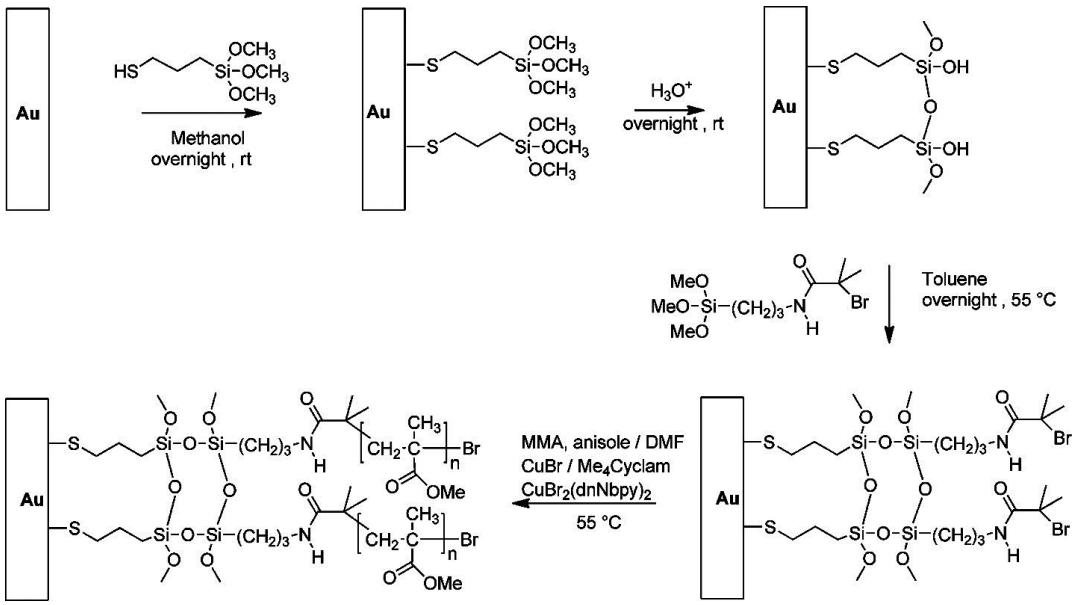

Figure 23. Surface-initiated polymerization of PMMA from crosslinked ATRP initiators on Au. Reprinted with permission from Ref.[97], copyright 2011 American Chemical Society. PMMA: Polymethylmethacrylate; ATRP: atom transfer radical polymerization.

The authors found that normal alkanethiols with ATRP initiator on gold led to the growth of thinner polymers compared to silane SAMs with ATRP initiator on a SiO_2 substrate due to the poor thermostability of uncrosslinked initiators. In contrast to a crosslinked polysiloxane primer layer, polymer brushes grown from ATRP initiators on Au reached the same thickness as on a SiO_2 substrate, as shown in Figure 24. Thanks to the highly stable Si-O bond of crosslinked silane-based SAMs, the novel ATRP initiator allowed SIP at higher temperatures of up to 100 °C, which provides polymer growth from less reactive monomers such as styrene and vinyl pyridine.

Compared to the aromatic thiol-based SAMs, homogeneous SIP from crosslinked silane-based alkanethiols is cost-efficient because it does not need an expensive e-beam lithography system for the crosslinking process. However, it is difficult to pattern silane-based SAMs since it has been reported that silanes are not compatible with microcontact printing techniques[16].

Surface passivation

GaAs is a promising III-V semiconductor material that is widely used in devices such as photovoltaics, light-emitting diodes, photonics, and radio frequency transistors, thanks to its high electron mobility and direct bandgap[105,106]. To date, GaAs solar cells have shown record-breaking conversion efficiencies, ~29% for single-junction cells[107]. However, GaAs can become oxidized in the ambient environment, and the oxide layer formed on GaAs can significantly decrease the solar cell efficiency[108]. Hence, surface passivation

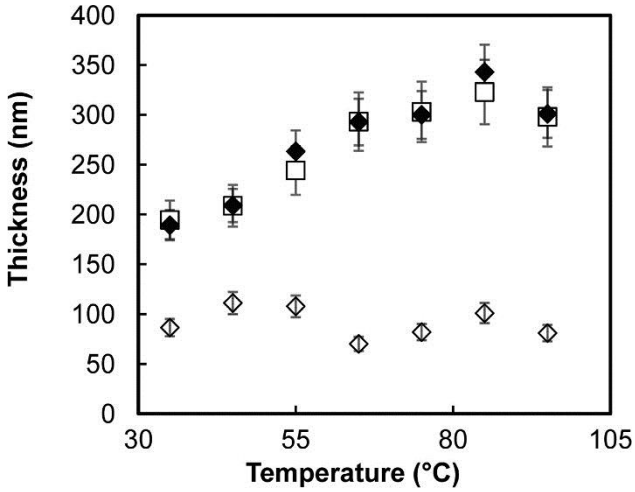

Figure 24. Temperature-dependent surface-initiated polymerization of MMA from various initiators; ◊ PMMA grown from a standard initiator; ♦ PMMA grown from the crosslinked initiator; and □ PMMA grown from a silane initiator on SiO_2. Reprinted with permission from Ref.[97], copyright 2011 American Chemical Society. PMMA: Polymethylmethacrylate; MMA: methyl methacrylate.

of GaAs devices to prevent oxidation and corrosion is the key to enhancing the durability and performance of GaAs devices. Because sulfur species can bind to both Ga and As atoms to passivate unsaturated binding sites and form a thin protective layer on a GaAs surface, scientists have attempted to use several sulfur compounds to passivate a GaAs surface, such as $(NH_4)_2S$, Na_2S, and normal alkanethiols[109,110]. However, when GaAs is treated with the first two inorganic salts, toxic H_2S is produced. Moreover, passivation layers on the GaAs surface formed by all three kinds of compounds are less than 2 nm thick, which means that oxygen can still diffuse into the protective film to oxidize the GaAs surface after 2 days[111].

In 1997, Kauffman and co-workers discovered that MPTMS SAM was a good candidate for GaAs surface passivation[99]. After years of development, MPTMS has been widely used in GaAs devices such as solar cells and GaAs-based sensors, and the process used for surface passivation has become efficient and mature[98]. As shown in Figure 25A-C, after hydrolysis in solutions of concentrated MPTMS and NH_4OH, the MPTMS monolayer formed on GaAs is crosslinked with other MPTMS molecules in the solution phase, which forms a 3D polysiloxane network. Finally, a relatively thick polymeric layer on the GaAs surface is generated, with the thickness of the resulting films ranging from 15 nm to 33 nm, which is controlled by varying the concentration of the MPTMS and NH_4OH solutions[98]. The results show that GaAs devices with MPTMS coatings show long-term stability in air or aqueous environments for at least 10 days without sacrificing their original performance.

Moreover, in 2002, Seitz and co-workers achieved polymerization of MPTMS in a solution sol-gel process for GaAs surface passivation[111]. In the follow-up research, this process was further developed to be used as an anti-corrosion coating for copper by Sui *et al.*[101]. Unlike the method introduced above, a polysiloxane network was formed by the polymerization of MPTMS in solution before being coated onto the copper surface.

CROSSLINKED BORONIC ACID-BASED SAMS

In 1994, Whiteside and co-workers utilized boronic acid-based alkanethiols to fabricate a crosslinked boronic anhydride surface[112]. Although this research was focused on boronic acid-based SAMs[113], subsequent research for boronic acid-based SAMs for crosslinking is limited. Additionally, there exists only

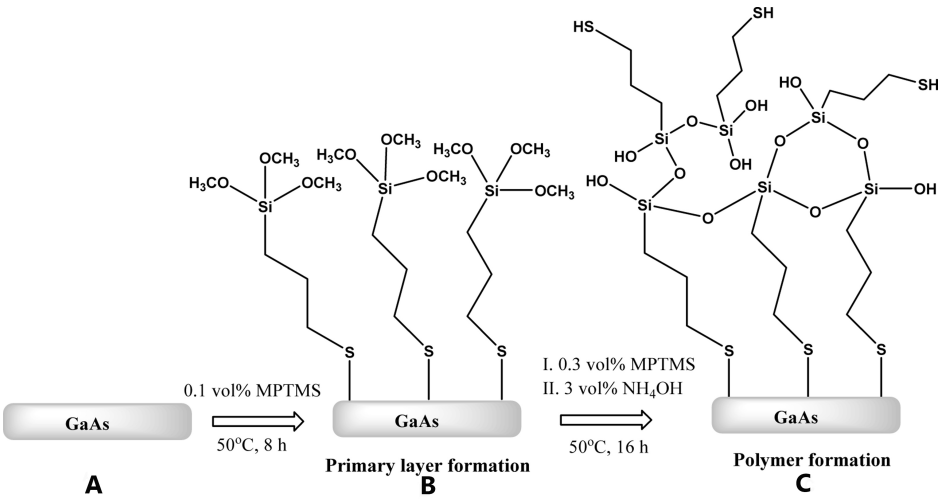

Figure 25. Schematic representation of an MPTMS coating on the surface of GaAs: (A) cleaned and etched GaAs sample, (B) primary layer formation, and (C) polymer formation. Reprinted with permission from Ref.[102], copyright 2016 American Chemical Society. MPTMS: (3-mercaptopropyl) trimethoxysilane.

limited research about the application of this kind of crosslinked SAM system.

A crosslinked boronic anhydride surface was first fabricated by the condensation of 11-mercaptoundecanyl-l-boronic acid, $HS(CH_2)_nB(OH)_2$ in dry hydrocarbon solvents, such as isooctane, or under vacuum, as shown in Figure 26[112]. This reaction is reversible, and the crosslinked film can be converted back into a pristine monolayer in aqueous ethanol. The author also found that in dry hydrocarbon solvents, $HS(CH_2)_nB(OH)_2$ molecules in the solution phase reversibly turn into trimers that adsorb onto gold and form a hydrophobic boroxine bilayer. The resulting hydrophobic bilayer can be converted into a hydrophilic monolayer again in aqueous ethanol. Similar to hydroxyl-terminated SAMs, both the $HS(CH_2)_nB(OH)_2$ SAM and its crosslinked film can couple with alkyltrichlorosilanes irreversibly, turning into a borosilicate network.

Applications

Thermally stable coatings

The thermal desorption results show that the crosslinked boronic anhydride SAM is five times more stable compared to the structurally analogous 11-hydroxyundecane-l-thiol at 147 °C. However, it is difficult to tune the thickness or crosslinked area of crosslinked boronic acid-based SAMs. Moreover, the formation of crosslinked boronic anhydride surface is reversible. These drawbacks hinder the application of crosslinked boronic acid-based SAMs compared to other crosslinked systems such as aromatic thiol-based SAMs.

CROSSLINKED SAMS REALIZED BY HYDROGEN BONDING

In addition to crosslinking with covalent bonding, another important type of crosslinked SAMs are SAMs with noncovalent interaction such as hydrogen bonding. Generally, the hydrogen bonding within these crosslinked SAMs arises from the amide functional group or carboxylic acid group in the tailgroups. In 1994, Rabolt and co-workers synthesized semifluorinated amidethiol, which was the first reported crosslinked SAM with hydrogen bonding, as shown in Figure 27A[114]. In a follow-up study, Whitesides and co-workers continued this research and synthesized a series of amidethiol SAMs, which were terminated with different functional groups, such as CH_3, OH, CF_3, COOH, *etc.*, as shown in Figure 27B[115]. In 1997, Sastry *et al.*[116] prepared a 4-carboxythiophenol SAM, with the carboxylic acid moieties forming a hydrogen-

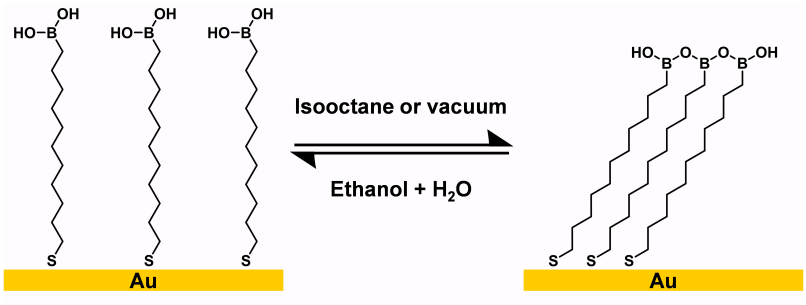

Figure 26. Schematic representation of a crosslinked boronic anhydride surface. Adapted from Ref.[112], copyright 1994 American Chemical Society.

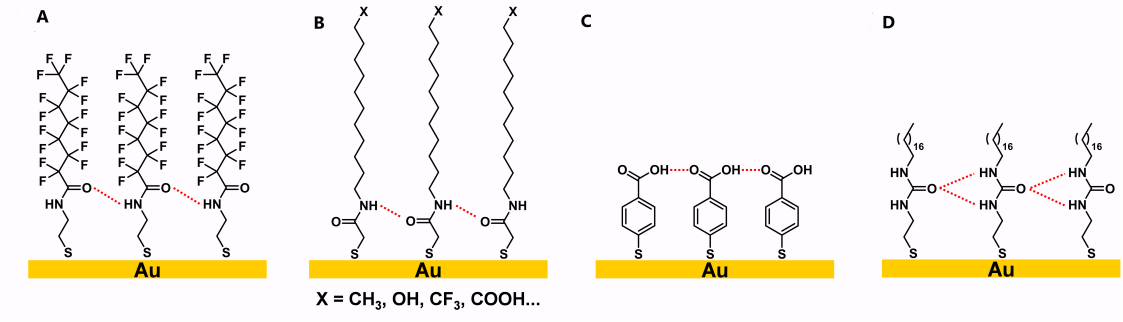

Figure 27. Structures of 4 different crosslinked SAMs realized by hydrogen bonding[114-117]. SAMs: Self-assembled monolayers.

bonding network at low pH, as shown in Figure 27C. In 2005, Kim *et al.*[117] synthesized SAMs with a urea moiety on gold, which formed a hydrogen-bonding network, as shown in Figure 27D.

When SAMs containing carboxylic acid, amide, and urea groups are absorbed on gold, hydrogen-bonding networks are formed spontaneously. In the case of the SAM containing a urea moiety in Figure 27D, infrared reflection-absorption (IRRA) spectra obtained for the SAM on gold show almost no amide I band, which appears at 1621 cm^{-1} in the spectra obtained for the bulk molecules[117]. This result proved that hydrogen bonding exists in the SAM network, which is composed of N-H and C=O bonds parallel to the surface, since only vibrations aligned with the surface normal appear in the IRRA spectra due to the metal-surface selection rule. In 2016, Thomas *et al.*[118] used STM to map the hydrogen-bonding networks formed in SAMs with an amide group. The submolecular-resolution STM images showed a linear pattern of molecule orientation (tilts) affected by hydrogen bonding, which further confirmed the existence of hydrogen bonding in the SAM network.

Applications

Selective binding of cations on surfaces

In the follow-up research, Liedberg and co-workers studied the thermal stability of SAMs influenced by hydrogen bonding, as measured by temperature-programmed desorption (TPD)[119]. They noted that SAMs with amide moieties show better thermostability compared to their normal alkanethiol analogs, with a temperature difference of 25 K for the thermodesorption, due to the hydrogen bonding. Moreover, Sastry *et al.*[116] studied the effect of a 4-carboxythiophenol SAM on the selective binding of Cd and Pb cations on surfaces. As shown in Figure 28, at low pH, the carboxylic acid groups at the interface are pronated and form a hydrogen-bonding network. They deprotonate and bind to cations in the form of

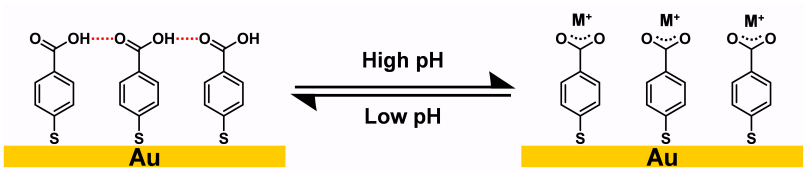

Figure 28. Schematic representation of 4-carboxythiophenol SAM on Au at low pH, and ion adsorption [M^+ = $Cd(OH)^+$ or $Pb(OH)^+$] at high pH. Adapted from Ref.[116], copyright 1997 American Chemical Society. SAM: Self-assembled monolayer.

$Cd(OH)^+$ or $Pb(OH)^+$ through an ion-exchange process. In addition, Rotello and co-workers investigated the position of the amide group in the alkyl chain in SAM-coated gold nanoparticles[120]. Their results showed that when the amide group is near the SAM interface, intermonolayer hydrogen bonding leads to the aggregation of nanoparticles.

CONCLUSION AND OUTLOOK

In this review, we highlighted a variety of crosslinked SAMs: (1) aromatic thiol-based SAMs; (2) olefinic- and acetylenic-based SAMs; (3) other aliphatic SAMs; (4) silane-based SAMs; (5) boronic acid-based SAMs; and (6) SAMs realized by hydrogen bonding. Their methods of formation including the conditions for crosslinking, the structures of the crosslinked products, and their interfacial properties were discussed. Furthermore, we highlighted the applications of such crosslinked SAMs in materials science, such as the fabrication of carbon nanomembranes, lithography, protective coatings, surface functionalization, and surface-initiated polymerization.

The rapid development in semiconductor industry has attracted increasing attention from scientists and engineers seeking to develop new methods to fabricate nanostructures for next-generation semiconductor chips. Although it remains difficult to achieve uniform deposition of SAMs at a 300-mm-wafer scale, and stability still limits the application of uncrosslinked SAMs under etching or epitaxy conditions, we believe that crosslinked SAMs are attractive candidates in future semiconductor manufacturing industries. Importantly, with less than 5-nanometer thicknesses, crosslinked SAMs can tolerate extreme UV photolithography and even X-ray lithography under nanofabrication conditions. We hope this review offers insight into the structure-property relationships of crosslinked SAMs, as well as inspires researchers toward the development of new types of SAMs with enhanced stabilities.

DECLARATIONS

Authors' contribution

Prepared the original draft: Yu T, Marquez MD, Tran HV
Edited the draft and added additional written content: Lee TR

Availability of data and materials

Not applicable.

Financial support and sponsorship

We thank the National Science Foundation (CHE-2109174), the Robert A Welch Foundation (Grant No. E-1320), and the Texas Center for Superconductivity at the University of Houston for the support.

Conflicts of interest

All authors declared that there are no conflicts of interest.

Ethical approval and consent to participate

Not applicable.

Consent for publication

Not applicable.

Copyright

© The Author(s) 2022.

REFERENCES

1. Nuzzo RG, Allara DL. Adsorption of bifunctional organic disulfides on gold surfaces. *J Am Chem Soc* 1983;105:4481-3. DOI
2. Bain CD, Troughton EB, Tao YT, Evall J, Whitesides GM, Nuzzo RG. Formation of monolayer films by the spontaneous assembly of organic thiols from solution onto gold. *J Am Chem Soc* 1989;111:321-35. DOI
3. Nuzzo RG, Zegarski BR, Dubois LH. Fundamental studies of the chemisorption of organosulfur compounds on gold(111). Implications for molecular self-assembly on gold surfaces. *J Am Chem Soc* 1987;109:733-40. DOI
4. Kim SH, Asay DB, Dugger MT. Nanotribology and MEMS. *Nano Today* 2007;2:22-9. DOI PubMed
5. Nuzzo RG. Biomaterials: Stable antifouling surfaces. *Nat Mater* 2003;2:207-8. DOI PubMed
6. Ruiz S, Chen CS. Microcontact printing: a tool to pattern. *Soft Matter* 2007;3:168-77. DOI PubMed
7. Wilbur JL, Kumar A, Kim E, Whitesides GM. Microfabrication by microcontact printing of self-assembled monolayers. *Adv Mater* 1994;6:600-4. DOI
8. Doms M, Feindt H, Kuipers WJ, et al. Hydrophobic coatings for MEMS applications. *J Micromech Microeng* 2008;18:055030. DOI
9. Yu T, Marquez MD, Zenasni O, Lee TR. Mimicking polymer surfaces using cyclohexyl- and perfluorocyclohexyl-terminated self-assembled monolayers. *ACS Appl Nano Mater* 2019;2:5809-16. DOI
10. Maboudian R, Ashurst W, Carraro C. Self-assembled monolayers as anti-stiction coatings for MEMS: characteristics and recent developments. *Sensors and Actuators A: Physical* 2000;82:219-23. DOI
11. Kasai T, Bhushan B, Kulik G, Barbieri L, Hoffmann P. Micro/nanotribological study of perfluorosilane SAMs for antistiction and low wear. *J Vac Sci Technol B* 2005;23:995. DOI
12. Bhushan B, Kasai T, Kulik G, Barbieri L, Hoffmann P. AFM study of perfluoroalkylsilane and alkylsilane self-assembled monolayers for anti-stiction in MEMS/NEMS. *Ultramicroscopy* 2005;105:176-88. DOI
13. Kim S, Yoo H. Self-assembled monolayers: versatile uses in electronic devices from gate dielectrics, dopants, and biosensing linkers. *Micromachines (Basel)* 2021;12:565. DOI PubMed PMC
14. Grönbeck H, Curioni A, Andreoni W. Thiols and disulfides on the Au(111) surface: the headgroup - gold interaction. *J Am Chem Soc* 2000;122:3839-42. DOI
15. Crudden CM, Horton JH, Ebralidze II, et al. Ultra stable self-assembled monolayers of N-heterocyclic carbenes on gold. *Nat Chem* 2014;6:409-14. DOI PubMed
16. Onclin S, Ravoo BJ, Reinhoudt DN. Engineering silicon oxide surfaces using self-assembled monolayers. *Angew Chem Int Ed Engl* 2005;44:6282-304. DOI PubMed
17. Delamarche E, Michel B, Kang H, Gerber C. Thermal stability of self-assembled monolayers. *Langmuir* 1994;10:4103-8. DOI PubMed
18. Ulman A. Formation and structure of self-assembled monolayers. *Chem Rev* 1996;96:1533-54. DOI PubMed
19. Allara DL, Parikh AN, Rondelez F. Evidence for a unique chain organization in long chain silane monolayers deposited on two widely different solid substrates. *Langmuir* 1995;11:2357-60. DOI
20. Srisombat L, Jamison AC, Lee TR. Stability: a key issue for self-assembled monolayers on gold as thin-film coatings and nanoparticle protectants. *Colloids and Surfaces A: Physicochemical and Engineering Aspects* 2011;390:1-19. DOI
21. Geyer W, Stadler V, Eck W, Zharnikov M, Gölzhäuser A, Grunze M. Electron-induced crosslinking of aromatic self-assembled monolayers: negative resists for nanolithography. *Appl Phys Lett* 1999;75:2401-3. DOI
22. Angelova P, Vieker H, Weber NE, et al. A universal scheme to convert aromatic molecular monolayers into functional carbon nanomembranes. *ACS Nano* 2013;7:6489-97. DOI PubMed
23. Turchanin A, Gölzhäuser A. Carbon nanomembranes from self-assembled monolayers: Functional surfaces without bulk. *Progress in Surface Science* 2012;87:108-62. DOI
24. Schmid M, Wan X, Asyuda A, Zharnikov M. Modification of self-assembled monolayers by electron irradiation: the effect of primary energy (10-500 eV). *J Phys Chem C* 2019;123:28301-9. DOI
25. Tong Y, Berdiyorov GR, Sinopoli A, Madjet ME, Esaulov VA, Hamoudi H. An estimation on the mechanical stabilities of SAMs by low energy Ar^+ cluster ion collision. *Sci Rep* 2021;11:12772. DOI PubMed PMC
26. Eck W, Stadler V, Geyer W, Zharnikov M, Gölzhäuser A, Grunze M. Generation of surface amino groups on aromatic self-assembled monolayers by low energy electron beams - a first step towards chemical lithography. *Adv Mater* 2000;12:805-8. DOI
27. Meyerbröker N, Zharnikov M. Modification of nitrile-terminated biphenylthiol self-assembled monolayers by electron irradiation and

related applications. *Langmuir* 2012;28:9583-92. DOI PubMed
28. Turchanin A, Käfer D, El-Desawy M, Wöll C, Witte G, Gölzhäuser A. Molecular mechanisms of electron-induced cross-linking in aromatic SAMs. *Langmuir* 2009;25:7342-52. DOI PubMed
29. Houplin J, Dablemont C, Sala L, Lafosse A, Amiaud L. Electron processing at 50 eV of terphenylthiol self-assembled monolayers: contributions of primary and secondary electrons. *Langmuir* 2015;31:13528-34. DOI PubMed
30. Amiaud L, Houplin J, Bourdier M, et al. Low-energy electron induced resonant loss of aromaticity: consequences on cross-linking in terphenylthiol SAMs. *Phys Chem Chem Phys* 2014;16:1050-9. DOI PubMed
31. Luo YR. Comprehensive handbook of chemical bond energies. New York: CRC Press; 2007. p. 50. DOI
32. Zharnikov M, Grunze M. Modification of thiol-derived self-assembling monolayers by electron and x-ray irradiation: scientific and lithographic aspects. *J Vac Sci Technol B* 2002;20:1793. DOI
33. Zhang X, Vieker H, Beyer A, Gölzhäuser A. Fabrication of carbon nanomembranes by helium ion beam lithography. *Beilstein J Nanotechnol* 2014;5:188-94. DOI PubMed PMC
34. Turchanin A, Schnietz M, El-Desawy M, Solak HH, David C, Gölzhäuser A. Fabrication of molecular nanotemplates in self-assembled monolayers by extreme-ultraviolet-induced chemical lithography. *Small* 2007;3:2114-9. DOI PubMed
35. Cabrera-Sanfelix P, Arnau A, Sánchez-Portal D. First-principles investigation of electron-induced cross-linking of aromatic self-assembled monolayers on Au(111). *Phys Chem Chem Phys* 2010;12:1578-84. DOI PubMed
36. Koch S, Kaiser CD, Penner P, et al. Amplified cross-linking efficiency of self-assembled monolayers through targeted dissociative electron attachment for the production of carbon nanomembranes. *Beilstein J Nanotechnol* 2017;8:2562-71. DOI PubMed PMC
37. Yildirim C, Füser M, Terfort A, Zharnikov M. Modification of aromatic self-assembled monolayers by electron irradiation: basic processes and related applications. *J Phys Chem C* 2017;121:567-76. DOI
38. Mrugalla A, Schnack J. Classical molecular dynamics investigations of biphenyl-based carbon nanomembranes. *Beilstein J Nanotechnol* 2014;5:865-71. DOI PubMed PMC
39. Ishida T, Hara M, Kojima I, et al. High resolution X-ray photoelectron spectroscopy measurements of octadecanethiol self-assembled monolayers on Au(111). *Langmuir* 1998;14:2092-6. DOI
40. Smith BW. Optical projection lithography. In Feldman M. Ed. Nanolithography. New York: Woodhead Publishing; 2014. p. 1-41. DOI
41. Altissimo M. E-beam lithography for micro-nanofabrication. *Biomicrofluidics* 2010;4:026503. DOI PubMed PMC
42. Groves TR. Electron beam lithography. In: Feldman M. Ed. Nanolithography. New York: Woodhead Publishing; 2014. P. 80-115. DOI
43. Tseng A, Kuan Chen, Chen C, Ma K. Electron beam lithography in nanoscale fabrication: recent development. *IEEE Trans Electron Packag Manufact* 2003;26:141-9. DOI
44. Gölzhäuser A, Eck W, Geyer W, et al. Chemical nanolithography with electron beams. *Adv Mater* ;13:803-6. DOI
45. Gölzhäuser A, Geyer W, Stadler V, et al. Nanoscale patterning of self-assembled monolayers with electrons. *J Vac Sci Technol B* 2000;18:3414. DOI
46. Barriet D. Fluorinated self-assembled monolayers: composition, structure and interfacial properties. *Current Opinion in Colloid & Interface Science* 2003;8:236-42. DOI
47. Frey S, Heister K, Zharnikov M, Grunze M. Modification of semifluorinated alkanethiolate monolayers by low energy electron irradiation. *Phys Chem Chem Phys* ;2:1979-87. DOI
48. Chesneau F, Hamoudi H, Schüpbach B, Terfort A, Zharnikov M. Modification of self-assembled monolayers of perfluoroterphenyl-substituted alkanethiols by low-energy electrons. *J Phys Chem C* 2011;115:4773-82. DOI
49. Frese N, Scherr J, Beyer A, et al. Multicomponent patterned ultrathin carbon nanomembranes by laser ablation. *Applied Surface Science* 2018;427:126-30. DOI
50. Turchanin A, El-desawy M, Gölzhäuser A. High thermal stability of cross-linked aromatic self-assembled monolayers: nanopatterning via selective thermal desorption. *Appl Phys Lett* 2007;90:053102. DOI
51. Beyer A, Godt A, Amin I, et al. Fully cross-linked and chemically patterned self-assembled monolayers. *Phys Chem Chem Phys* 2008;10:7233-8. DOI PubMed
52. Tran KT, Nguyen TD. Lithography-based methods to manufacture biomaterials at small scales. *Journal of Science: Advanced Materials and Devices* 2017;2:1-14. DOI
53. Turchanin A, Gölzhäuser A. Carbon nanomembranes. *Adv Mater* 2016;28:6075-103. DOI PubMed
54. Kankate L, Aguf A, Großmann H, et al. Vapor phase exchange of self-assembled monolayers for engineering of biofunctional surfaces. *Langmuir* 2017;33:3847-54. DOI PubMed
55. Turchanin A, Tinazli A, El-desawy M, et al. Molecular self-assembly, chemical lithography, and biochemical tweezers: a path for the fabrication of functional nanometer-scale protein arrays. *Adv Mater* 2008;20:471-7. DOI
56. Meyerbröker N, Li Z, Eck W, Zharnikov M. Biocompatible nanomembranes based on pegylation of cross-linked self-assembled monolayers. *Chem Mater* 2012;24:2965-72. DOI
57. Chesneau F, Terfort A, Zharnikov M. Nickel deposition on fluorinated, aromatic self-assembled monolayers: chemically induced cross-linking as a tool for the preparation of well-defined top metal films. *J Phys Chem C* 2014;118:11763-73. DOI
58. Kuang J, Messersmith PB. Universal surface-initiated polymerization of antifouling zwitterionic brushes using a mussel-mimetic peptide initiator. *Langmuir* 2012;28:7258-66. DOI PubMed PMC

59. Schmelmer U, Jordan R, Geyer W, et al. Surface-initiated polymerization on self-assembled monolayers: amplification of patterns on the micrometer and nanometer scale. *Angew Chem Int Ed Engl* 2003;42:559-63. DOI PubMed
60. Schmelmer U, Paul A, Küller A, et al. Nanostructured polymer brushes. *Small* 2007;3:459-65. DOI PubMed
61. Amin I, Steenackers M, Zhang N, et al. Polymer carpets. *Small* 2010;6:1623-30. DOI PubMed
62. Eck W, Küller A, Grunze M, Völkel B, Gölzhäuser A. Freestanding nanosheets from crosslinked biphenyl self-assembled monolayers. *Adv Mater* 2005;17:2583-7. DOI
63. Angelova P, Gölzhäuser A. Carbon nanomembranes. *Physical Sciences Reviews* 2017:2. DOI
64. Schnietz M, Turchanin A, Nottbohm CT, et al. Chemically functionalized carbon nanosieves with 1-nm thickness. *Small* 2009;5:2651-5. DOI PubMed
65. Kruk M, Neumann C, Frey M, Kozieł K, Turchanin A, Cyganik P. Odd-even effect in electron beam irradiation of hybrid aromatic-aliphatic self-assembled monolayers of fatty acid. *J Phys Chem C* 2021;125:9310-8. DOI
66. Zheng Z, Zhang X, Neumann C, et al. Hybrid van der Waals heterostructures of zero-dimensional and two-dimensional materials. *Nanoscale* 2015;7:13393-7. DOI PubMed
67. Turchanin A. Graphene growth by conversion of aromatic self-assembled monolayers. *ANNALEN DER PHYSIK* 2017;529:1700168. DOI
68. Yang Y, Dementyev P, Biere N, et al. Rapid water permeation through carbon nanomembranes with sub-nanometer channels. *ACS Nano* 2018;12:4695-701. DOI PubMed
69. Zhang X, Marschewski E, Penner P, et al. Large-area all-carbon nanocapacitors from graphene and carbon nanomembranes. *ACS Nano* 2018;12:10301-9. DOI PubMed
70. Woszczyna M, Winter A, Grothe M, et al. All-carbon vertical van der Waals heterostructures: non-destructive functionalization of graphene for electronic applications. *Adv Mater* 2014;26:4831-7. DOI PubMed
71. Matei DG, Weber NE, Kurasch S, et al. Functional single-layer graphene sheets from aromatic monolayers. *Adv Mater* 2013;25:4146-51. DOI PubMed
72. Weber NE, Wundrack S, Stosch R, Turchanin A. Direct growth of patterned graphene. *Small* 2016;12:1440-5. DOI PubMed
73. Turchanin A, Beyer A, Nottbohm CT, et al. One nanometer thin carbon nanosheets with tunable conductivity and stiffness. *Adv Mater* 2009;21:1233-7. DOI
74. Kunjuzwa N, Nthunya LN, Nxumalo EN, Mhlanga SD. The use of nanomaterials in the synthesis of nanofiber membranes and their application in water treatment. In Advanced Nanomaterials for Membrane Synthesis and its Applications, Lau, W.-J.; Ismail, A. F.; Isloor, A.; Al-Ahmed, A., Eds.; Elsevier, 2019. p. 101-25. DOI
75. Araújo LCA, Costa LP. Functionalized carbon nano-membranes based devices for water purification technology. In: Environmental Applications of Carbon Nanomaterials-Based Devices. 2021. p. 331-46. DOI
76. Dementyev P, Wilke T, Naberezhnyi D, Emmrich D, Gölzhäuser A. Vapour permeation measurements with free-standing nanomembranes. *Phys Chem Chem Phys* 2019;21:15471-7. DOI PubMed
77. Yang Y, Hillmann R, Qi Y, et al. Ultrahigh ionic exclusion through carbon nanomembranes. *Adv Mater* 2020;32:e1907850. DOI PubMed
78. Weston M, Tjandra AD, Chandrawati R. Tuning chromatic response, sensitivity, and specificity of polydiacetylene-based sensors. *Polym Chem* 2020;11:166-83. DOI
79. Reppy MA, Pindzola BA. Biosensing with polydiacetylene materials: structures, optical properties and applications. *Chem Commun (Camb)* 2007;42:4317-38. DOI PubMed
80. Batchelder DN, Evans SD, Freeman TL, Haeussling L, Ringsdorf H, Wolf H. Self-assembled monolayers containing polydiacetylenes. *J Am Chem Soc* 1994;116:1050-3. DOI
81. Cai M, Mowery MD, Menzel H, Evans CE. Fabrication of extended conjugation length polymers within diacetylene monolayers on au surfaces: influence of UV exposure time. *Langmuir* 1999;15:1215-22. DOI
82. Takajo D, Sudoh K. Mechanism of chain polymerization in self-assembled monolayers of diacetylene on the graphite surface. *Langmuir* 2019;35:2123-8. DOI PubMed
83. Wu F, Bhupathiraju NVSDK, Brown A, Liu Z, Drain CM, Batteas JD. Mechanical and electronic properties of diacetylene and polydiacetylene self-assembled monolayers on Au(111). *J Phys Chem C* 2020;124:4081-9. DOI
84. Menzel H, Mowery MD, Cai M, Evans CE. Vertical positioning of internal molecular scaffolding within a single molecular layer. *J Phys Chem B* 1998;102:9550-6. DOI
85. Kim T, Crooks RM, Tsen M, Sun L. Polymeric self-assembled monolayers. 2. Synthesis and characterization of self-assembled polydiacetylene mono- and multilayers. *J Am Chem Soc* 1995;117:3963-7. DOI
86. Kim T, Chan KC, Crooks RM. Polymeric self-assembled monolayers. 4. chemical, electrochemical, and thermal stability of ω-functionalized, self-assembled diacetylenic and polydiacetylenic monolayers. *J Am Chem Soc* 1997;119:189-93. DOI
87. Ford JF, Vickers TJ, Mann CK, Schlenoff JB. Polymerization of a thiol-bound styrene monolayer. *Langmuir* 1996;12:1944-6. DOI
88. Chan KC, Kim T, Schoer JK, Crooks RM. Polymeric self-assembled monolayers. 3. Pattern transfer by use of photolithography, electrochemical methods, and an ultrathin, self-assembled diacetylenic resist. *J Am Chem Soc* 1995;117:5875-6. DOI
89. Yang W, Ella-Menye JR, Liu S, et al. Cross-linked carboxybetaine SAMs enable nanoparticles with remarkable stability in complex media. *Langmuir* 2014;30:2522-9. DOI PubMed
90. Chien HW, Cheng PH, Chen SY, Yu J, Tsai WB. Low-fouling and functional poly(carboxybetaine) coating via a photo-crosslinking

process. *Biomater Sci* 2017;5:523-31. DOI PubMed

91. Wang Y, Sun Y, Ding X, Liang J, Cao X, Tian Z. A combined electro- and photo-chemical approach to repeatedly fabricate two-dimensional molecular assemblies. *Electrochimica Acta* 2017;246:823-9. DOI
92. Olsen C, Rowntree PA. Bond-selective dissociation of alkanethiol based self-assembled monolayers adsorbed on gold substrates, using low-energy electron beams. *The Journal of Chemical Physics* 1998;108:3750-64. DOI
93. Zharnikov M, Geyer W, Gölzhäuser A, Frey S, Grunze M. Modification of alkanethiolate monolayers on Au-substrate by low energy electron irradiation: Alkyl chains and the S/Au interface. *Phys Chem Chem Phys* ;1:3163-71. DOI
94. Zharnikov M, Frey S, Heister K, Grunze M. Modification of alkanethiolate monolayers by low energy electron irradiation: dependence on the substrate material and on the length and isotopic composition of the alkyl chains. *Langmuir* 2000;16:2697-705. DOI
95. Huels MA, Dugal P, Sanche L. Degradation of functionalized alkanethiolate monolayers by 0-18 eV electrons. *The Journal of Chemical Physics* 2003;118:11168-78. DOI
96. Waske PA, Meyerbröker N, Eck W, Zharnikov M. Self-assembled monolayers of cyclic aliphatic thiols and their reaction toward electron irradiation. *J Phys Chem C* 2012;116:13559-68. DOI
97. Saha S, Bruening ML, Baker GL. Facile synthesis of thick films of poly(methyl methacrylate), poly(styrene), and poly(vinyl pyridine) from Au surfaces. *ACS Appl Mater Interfaces* 2011;3:3042-8. DOI PubMed PMC
98. Tkachev M, Anand-kumar T, Bitler A, Guliamov R, Naaman R. Enabling long-term operation of GaAs-based sensors. *ENG* 2013;05:1-12. DOI
99. Hou T, Greenlief CM, Keller SW, Nelen L, Kauffman JF. Passivation of GaAs (100) with an adhesion promoting self-assembled monolayer. *Chem Mater* 1997;9:3181-6. DOI
100. Masi G, Balbo A, Esvan J, et al. X-ray photoelectron spectroscopy as a tool to investigate silane-based coatings for the protection of outdoor bronze: the role of alloying elements. *Applied Surface Science* 2018;433:468-79. DOI
101. Sui W, Zhao W, Zhang X, Peng S, Zeng Z, Xue Q. Comparative anti-corrosion properties of alkylthiols SAMs and mercapto functional silica sol-gel coatings on copper surface in sodium chloride solution. *J Sol-Gel Sci Technol* 2016;80:567-78. DOI
102. Sharma H, Moumanis K, Dubowski JJ. pH-dependent photocorrosion of GaAs/AlGaAs quantum well microstructures. *J Phys Chem C* 2016;120:26129-37. DOI
103. Savard S, Blanchard L, Léonard J, Prud'homme RE. Hydrolysis and condensation of silanes in aqueous solutions: hydrolysis and condensation of silanes in aqueous solutions. *Polym Compos* 1984;5:242-9. DOI
104. Itoh M, Nishihara H, Aramaki K. A chemical modification of alkanethiol Self-assembled monolayers with alkyltrichlorosilanes for the protection of copper against corrosion. *J Electrochem Soc* 1994;141:2018-23. DOI
105. Liu i, Ma K, Mou S, Meng F. A review of recent power amplifier IC. In: 2017 10th Global Symposium on Millimeter-Waves. 2017. p. 87-91. DOI
106. Asadirad M, Rathi M, Pouladi S, et al. III-V thin-film photovoltaic solar cells based on single-crystal-like GaAs grown on flexible metal tapes. In: 2016 IEEE 43rd Photovoltaic Specialists Conference (PVSC); IEEE: Portland, OR. 2016. p. 1954-6. DOI
107. Green MA, Hishikawa Y, Dunlop ED, Levi DH, Hohl-ebinger J, Ho-baillie AW. Solar cell efficiency tables (version 51). *Prog Photovolt Res Appl* 2018;26:3-12. DOI
108. Sheldon MT, Eisler CN, Atwater HA. GaAs Passivation with trioctylphosphine sulfide for enhanced solar cell efficiency and durability. *Adv Energy Mater* 2012;2:339-44. DOI
109. Carpenter MS, Melloch MR, Lundstrom MS, Tobin SP. Effects of Na_2S and $(NH_4)_2S$ edge passivation treatments on the dark current-voltage characteristics of GaAs. *pn* ;52:2157-9. DOI
110. Sheen CW, Shi JX, Maartensson J, Parikh AN, Allara DL. A new class of organized self-assembled monolayers: alkane thiols on gallium arsenide(100). *J Am Chem Soc* 1992;114:1514-5. DOI
111. Kirchner C, George M, Stein B, Parak W, Gaub H, Seitz M. Corrosion protection and long-term chemical functionalization of gallium arsenide in an aqueous environment. *Adv Funct Mater* ;12:266. DOI
112. Carey RI, Folkers JP, Whitesides GM. Self-assembled monolayers containing .omega.-mercaptoalkyl boronic acids adsorbed onto gold form a highly cross-linked, thermally stable borate glass surface. *Langmuir* 1994;10:2228-34. DOI
113. Fabre B, Hauquier F. Boronic acid-functionalized oxide-free silicon surfaces for the electrochemical sensing of dopamine. *Langmuir* 2017;33:8693-9. DOI PubMed
114. Lenk TJ, Hallmark VM, Hoffmann CL, et al. Structural investigation of molecular organization in self-assembled monolayers of a semifluorinated amidethiol. *Langmuir* 1994;10:4610-7. DOI
115. Tam-chang S, Biebuyck HA, Whitesides GM, Jeon N, Nuzzo RG. Self-assembled monolayers on gold generated from alkanethiols with the structure RNHCOCH2SH. *Langmuir* 1995;11:4371-82. DOI
116. Sastry M, Patil V, Mayya KS. Selective binding of divalent cations at the surface of self-assembled monolayers of an aromatic bifunctional molecule studied on a quartz crystal microbalance. *J Phys Chem B* 1997;101:1167-70. DOI
117. Kim JH, Shin HS, Kim SB, Hasegawa T. Hydrogen-bonding networks of dialkyl disulfides containing the urea moiety in self-assembled monolayers. *Langmuir* 2004;20:1674-9. DOI
118. Thomas JC, Goronzy DP, Dragomiretskiy K, et al. Mapping buried hydrogen-bonding networks. *ACS Nano* 2016;10:5446-51. DOI PubMed
119. Valiokas R, Östblom M, Svedhem S, Svensson SCT, Liedberg B. Thermal stability of self-assembled monolayers: influence of

lateral hydrogen bonding. *J Phys Chem B* 2002;106:10401-9. DOI

120. Boal AK, Rotello VM. Intra - and inter monolayer hydrogen bonding in amide-functionalized alkanethiol self-assembled monolayers on gold nanoparticles. *Langmuir* 2000;16:9527-32. DOI